







## Geology and hydrothermal alteration of the Santa Bárbara polymetallic deposit (Cu, Zn, Pb, Ag, Au): Insights into Ediacaran-Cambrian rift system evolution, Camaquã Basin, southern Brazil

Felipe Brito Mapa<sup>1,2,\*</sup> , Bruno Boito Turra<sup>1</sup> , João Luis Carneiro Naletto<sup>1</sup> , Rafael G. Landa Lazaro<sup>1</sup>,  
Guilherme Iolino Troncon Guerra<sup>1</sup> 

<sup>1</sup>Geological Survey of Brazil (SGB), Rua Costa, 55, São Paulo, São Paulo-SP, Brazil, CEP: 01304-010

<sup>2</sup>Programa de Pós-Graduação em Recursos Minerais e Hidrogeologia, Departamento de Geologia Sedimentar e Ambiental, Instituto de Geociências, Universidade de São Paulo, Rua do Lago, 562 – Cidade Universitária, Butantã, São Paulo-SP, Brazil, CEP: 05508-080

### Abstract

The Santa Bárbara deposit is a small polymetallic target (Cu, Zn, Pb, Au, Ag) located northwest of the Ediacaran Caçapava do Sul granite, near the namesake city, in the Sul-Riograndense shield. It is genetically linked to other two historical copper occurrences of the Cerro dos Andradas fault zone, the Primavera and Andrada deposits. This study explores the Cerro dos Andradas fault zone occurrences in the context of the tectonic evolution of the Ediacaran Camaquã rift system, focusing on the geological and hydrothermal characterization of the Santa Bárbara deposit. Mainly hosted in metamorphic rocks (Passo do Feio Complex) these occurrences have not been considered products of Camaquã basin evolution, unlike the other major mineralization of the region. The data were obtained by fieldwork, petrographic analysis of thin sections, and mineral reflectance spectroscopy of core samples, alongside geochemical and geological data acquired from a mineral exploration company. The mineralization are mainly hosted in the damage zone of a master fault of the Camaquã Basin (Andradas fault). The fault's NNE-SSW orientation is parallel to the mylonitic foliation of the footwall rocks, which comprise a metavolcano-sedimentary belt (Passo do Feio Complex) developed in the western wall of the granitic pluton. The host rocks include subvolcanic and volcanic lithotypes (basalt and andesite) of the hanging wall block of the Andradas Fault, related to the Bom Jardim Group. The results indicate that the mineralized veins consist of chalcopyrite, bornite, sphalerite, galena, quartz, calcite, ankerite, gypsum, and barite, with concentrations up to 0.8% copper, 0.6% zinc, and 0.3% lead, as well as significant gold and silver concentrations. Together with the definition of hydrothermal processes near the ore (carbonatization and argillization), these findings support the interpretation of an epithermal mineral system for the Cerro dos Andradas fault related deposits, similar to those proposed for other deposits in the Camaquã Basin.

### Article Information

Publication type: Research papers

Received 3 October 2024

Accepted 4 June 2025

Online pub. 11 June 2025

Editor: Maria José Mesquita

#### Keywords:

Copper  
Epithermal Deposit  
Master Fault  
Damage Zone  
Cerro dos Andradas

\*Corresponding author

Felipe Brito Mapa

E-mail address: [felipe.mapa@sgb.gov.br](mailto:felipe.mapa@sgb.gov.br)

### Accepted manuscript – Uncorrected pre-proof

This is a PDF file containing an unedited and non-definitive version of a manuscript that has been accepted for publication by the **Journal of the Geological Survey of Brazil – JGSB**, which serves to provide early visibility of the article. Being an uncorrected pre-proof version, errors may appear during the production process (language review, formatting and proof review), and these can affect the final content of the article and all legal disclaimers (<https://jgsb.sgb.gov.br/index.php/journal/6>).



## 1. Introduction

The Camaquã Basin is one of the main geological features of the Southern Riograndense Shield. Its evolution is linked to an active rift system that lasted for tens of millions of years during the Ediacaran and Cambrian periods (Almeida et al., 2010). This region is known for its extensive and well-preserved volcanic-sedimentary deposits, which show significant mineral potential for base (Cu, Pb, Zn) and precious (Au, Ag) metals. There are hundreds of known occurrences, particularly the Uruguai and São Luiz deposits in the Camaquã mining district, which are estimated to contain reserves of approximately 28 million tons at 1.05% Cu (Toniolo et al., 2010).

The relationship between the tectonic evolution of the Camaquã Basin and copper metallogeny has been established since early research. Ribeiro et al. (1966) and Ribeiro (1978) identify the structural, stratigraphic and lithological controls on mineralization. NE-SW faults primarily govern most mineral occurrences and influence the structural compartmentalization of the basin's volcanic and sedimentary records. The stratigraphic control is defined about a specific sedimentary unit, dating the mineralizing event to the "pre-Santa Bárbara Formation" (now the Guaritas Group). The lithological control is linked to the predominantly andesitic volcanism of the "Crespos Formation" (now the Hilário Formation).

Most metallogenic models link base metal occurrences in the South Rio Grande Shield to the evolution of the Camaquã Basin, connecting them to contemporary magmatic events (volcanism and granitogenesis). Although distinct models have been proposed for the Uruguai, São Luiz, and Santa Maria deposits (Ribeiro, 1991; Badi and Gonzales, 1988), the prevailing theory today is that they originated from a magmatic-hydrothermal process within an epithermal system (Melcher and Mau, 1960; Misi et al., 1999; Bettencourt, 1972; Remus et al., 2000a; Laux et al., 2005; Renac et al., 2014; Brito et al., 2023). Similar to other occurrences and mines in the region, such as Cerro dos Martins (Toniolo et al., 2004) and Seival (Toniolo et al., 2010; Mexias et al., 2007; Lopes et al., 2018), these mineralization are found within volcanic-sedimentary successions of the Camaquã Supergroup. Consequently, they are intrinsically linked to the evolution of the Camaquã Basin.

Significant copper deposits in the South Rio Grandense Shield are found near the Caçapava do Sul Granite. At Cerro dos Andradas, located between the granite to the east and the volcanic and sedimentary rocks of the Camaquã Supergroup to the west, the notable deposits include Primavera, Andradas, and Santa Bárbara. (Passos et al. 1959; Ribeiro 1978; Remus and Hartman 1997; Remus et al. 2000a). Passos et al. (1959) linked these deposits genetically, estimating a total reserve of 650,000 tons at 0.7% copper. Recent estimates indicate the Andradas deposit holds 22 million tons at 0.4% copper, with some high-grade intervals reaching up to 2.55% copper (Aguia, 2021).

The copper mineralization in these deposits are hosted in metamorphic basement rocks (Passo do Feio Complex, Bitencourt, 1983). Remus et al. (2000b) link their genesis to the mixing of magmatic fluids from the Caçapava Granite with formation fluids from the Passo do Feio Formation. They compare the mineralization in the Passo do Feio Formation (Cerro dos Andradas and others) with those in the Camaquã Supergroup (Uruguai and Santa Maria), suggesting ages of 594 Ma and 562 Ma, respectively. Although these ages align

with the formation of the Camaquã Basin, the authors propose distinct sources for these deposits. This has led researchers to connect the genesis of Passo Feio deposits to the evolution of the São Gabriel arc (e.g. Remus et al. 2000, Laux et al, 2021 Hoerlle et al, 2023), thereby distinguishing them from the evolution of the Camaquã Basin.

On the other hand, Martins et al (2010) recognize the hosted zone of the Primavera, Andradas and Santa Barbara deposits as the Cerro dos Andradas Shear Zone. They highlight a pattern of alternation between metabasic and granitic mylonites protolith throughout the structure, with deformation rates varying from protomylonites to ultramylonites. The authors suggest that the uplift of Caçapava do Sul High resulted from the vertical reactivation of this shear zone. Consequently, since the mineralization in the Cerro dos Andradas are linked to this vertical movement phase within the fault zone created after the mylonitic deformation, **these occurrences are likely** younger than the deformation of the Passo do Feio Formation and the formation of the Caçapava do Sul granite. Thus, they may be associated with the evolution of the Camaquã Basin.

This study examines the Cerro dos Andradas fault related occurrences in the context of the Ediacaran rift system, with a focus on the geological and hydrothermal characterization of the Santa Barbara deposit. Detailed analysis of hydrothermal mineral paragenesis in base metal deposits hosted in pre-Ediacaran basement rocks and shear zones may help establish the connection between the active tectonic regime and the source of base metal mineralizing fluids.

## 2. Geological setting

The metallogenesis of the Santa Bárbara Deposit is linked to the tectonic evolution of the Camaquã Basin (Ediacaran-Cambrian) and the post-collisional magmatism (Ediacaran) of the Dom Feliciano belt. The pre-Ediacaran basement primarily consists of Tonian-Cryogenian metamorphic and igneous rocks, related to the pre- and syn-collisional phases of the Brazilian orogeny in the São Gabriel and Tijucas terrains (see De Toni et al. 2023 and references).

The Camaquã Basin is a rift system active for about 50 million years (approximately 590 to 540 Ma) and consists of three volcano-sedimentary sequences: the Bom Jardim, Santa Bárbara, and Guaritas Groups, separated by discordances (Fragoso Cesar et al. 2000; Paim et al. 2000; Almeida et al. 2010; Almeida et al. 2012; Janikian et al. 2012; Paim et al. 2014). The Maricá Group, the basal unit of the Camaquã Supergroup, is classified as a "pre-rift" succession because it lacks fault boundaries and associated volcanism (Paim et al. 2000; Paim et al. 2014). The rift system has a general NNE-SSW orientation and is divided into three depositional troughs: the Eastern, Central, and Western sub-basins, separated by two basement highs (Figure 1A), the Caçapava do Sul and Santana da Boa Vista highs (Fragoso-Cesar et al., 2000).

Stratigraphic, paleocurrent, and provenance data indicate that the Caçapava do Sul High was active during the sedimentation of the Santa Bárbara Group and served as a source area for the Pedra do Segredo Formation top unit (Fambrini et al. 2006; Marconato et al. 2010). Conglomeratic alluvial fan deposits near the basin's edge fault indicate syn-sedimentary tectonic activity and the nucleation of a master fault during the final uplift stages (Fambrini et al. 2006, Marconato et al. 2010). Siliciclastic continental deposits make

up the sedimentary fill of the sub-basins.

The volcanic record consists of three units, from base to top: andesites of the Hilário Formation (approximately 590 Ma; Remus et al. 1999, Janikian et al. 2012), rhyolites of the Acampamento Velho Formation (580 to 540 Ma; Sommer et al. 2005, Janikian et al. 2008, Almeida et al. 2012, Matte et al. 2016), and basalts of the Rodeio Velho Formation (547 to 535 Ma; Almeida et al. 2010, Almeida et al. 2012). Volcanism also occurs beyond the rift's depositional troughs, extending to the adjacent Ramada and Taquarembó plateaus (Wildner et al. 2002, Sommer et al. 2006, Matte et al. 2016, Matte et al. 2021).

The Caçapava do Sul granite pluton is primarily composed of granodiorite, monzogranite, and syenogranite, with the latter two being the most abundant (Nardy and Bittencourt, 1989; Hoerlle et al. 2023). It has an elongated N-S geometry, displaying mylonitic textures at its edges and parallel contacts with the enclosing rock foliation, supporting its classification as a syn-kinematic intrusion (Nardy & Bittencourt, 1989; Fernandes et al. 1992; Costa et al. 1995; De Toni & Costa, 2024). Its crystallization age is around 570 Ma (Remus et al. 2000; Hoeller et al. 2023), correlating with the age range of the predominantly acid volcanism of the Acampamento Velho Formation (e.g., Lima et al. 2007; Janikian et al. 2012; Matte et al. 2016). Thus, the Caçapava do Sul granite, often linked to a "post-collisional" context (e.g., Bittencourt & Nardi 2000; De Toni et al. 2023), can also be viewed as the plutonic counterpart to the magmatism associated with rift system evolution (e.g., Janikian et al. 2008; Paim et al. 2014).

The metamorphic rocks surrounding the granite are mapped as the "Passo Feio Formation" since the pioneering work of Ribeiro et al. (1966). Due to their lithological diversity, Bittencourt (1989) refers to this unit as a "Complex," considered the host for the granite intrusion. There are different interpretations regarding protolith and geotectonic environments. Remus et al. (2000a) describe it as a metavolcano-sedimentary sequence representing an ancient basin that experienced regional metamorphism. In Cerro dos Andradas, Martins et al. (2010) identify a shear zone characterized by the concurrent mylonitization of the granite and the surrounding metabasic rocks. Battisti et al. (2023) dated zircons from metavolcanic rocks, yielding an age of 580 Ma, while dating of metamorphism in "metapelites" indicates an age of 570 Ma (Battisti et al., 2024). These ages are chronologically correlated with the Caçapava do Sul pluton and the volcanic activity in the Camaquã Basin (Acampamento Velho Formation). Tonian ages (~800 Ma) in detrital zircons, considered maximum sedimentation ages in metapelites, link the Passo Feio rocks to the Tonian units of the "São Gabriel Block" (Remus et al., 2000a; Lopez et al. 2015; Phillip et al. 2021). Souza (2020) links this ages to the Porongos belt located to the east side of Shield.

The mineralization studied here are located on the western edge of the Caçapava do Sul High, hosted within a shear zone at the tectonic contact between the Caçapava do Sul Granite to the east and sedimentary and volcanic rocks (Camaquã Supergroup) to the west (Figure 1B). Metasomatism and hydrothermal activity associated with the granite magmatism are linked to the region's metallogensis, resulting in epithermal systems (Remus et al. 2000a) and skarnitization of surrounding dolomitic rocks (Hoerlle et al. 2023), primarily occurring on the eastern edge of the pluton.

Epithermal mineralization systems are also reported in the Hilário volcanism and the Lavras do Sul granite (Mexias et al. 2007; Fontana et al. 2017; Fontana et al. 2019).

Figure 1: Location of the study area. (A) Regional tectonic location map (modified from Ribeiro, 1966, 1978; DNPM, 1989; Frago Cesar et al., 2000; CPRM, 2006; Almeida et al., 2012; Laux et al., 2021). (B) Local geological map (modified from Porcher et al., 1995).

### 3. Materials and methods

This study is based on fieldwork, sampling, and analyses of petrography and mineral reflectance spectroscopy conducted on drill core samples from the Santa Bárbara deposit, as part of an institutional project by the Geological Service of Brazil (SGB-CPRM). A total of 820 meters from nine different drill holes were examined, resulting in 37 polished thin sections and 1,033 VNIR-SWIR spectral signatures. The analyzed samples, drilling details and location are provided in Table 1.

Table 1: Location and drilling information for the drill cores used to describe the Santa Bárbara deposit

Mining Ventures Company donated the drill core collection and is accessible in the SGB-CPRM rock deposits (*Litoteca*) network. In addition to the descriptions and analysis conducted in this study, whole rock geochemical data and drill descriptions from related reports were also integrated.

The petrographic analysis in transmitted and reflected light were carried out at the Petrography Laboratory of the São Paulo Regional Superintendence of the SGB-CPRM, using an Olympus BX51 petrographic microscope with an attached camera, and at GeoFluid Laboratory of the Institute of Geosciences of the University of São Paulo (IGc-USP), using the Leica DM2700P petrographic microscope with a Leica DFC7000T digital camera.

The reflectance spectroscopy (RS) analysis were conducted at the *Litoteca* of Caçapava do Sul of the SGB-CPRM, using the ASD Fieldspec-3 Hi-Res spectroradiometer. This instrument captures mineral signatures across 2,151 bands, covering wavelengths from the visible to the short-wave infrared (VNIR-SWIR; 350 to 2500 nm).

The spectra were collected using a 20 mm diameter contact probe and a scanning method. Readings were taken every meter along the sample, focusing on specific points that reflected compositional, textural, and structural variations of interest.

The Mineralogical interpretation was based on visually inspecting the shape and specific wavelengths of diagnostic absorption features in the spectral signatures. This analysis utilized ENVI® and TSG™ Pro software, and reference mineral libraries (e.g., Hunt & Salisbury, 1970, 1971; Hunt et al., 1971a, 1971b; Hunt & Ashley, 1979; Clark et al., 1990; Clark, 1999; Pontual et al., 2008; Kokaly et al., 2017). The analysis focused on specific absorption features in selected spectra to investigate potential physical and chemical variations in the minerals, with results integrated into existing geological information.

The chemical data on trace elements in the whole rock was carried out by a laboratory contracted by the donor company (Intertek Laboratory) using the procedures of drying, crushing, homogenizing, quartering and pulverizing 1 kg of

sample in a 95% steel mill (200 mesh), determination of the chemical elements by four acids and ICP-OES reading. Gold was determined by the fusion of 50g of the pulverized sample by Atomic Absorption Fire Assay.

Spatial data processing, organization, and visualization were performed using ArcGIS Pro software, including drillhole management, base mapping, and integration of geological data. The three-dimensional modeling was conducted using Leapfrog Geo (v. 2023.2), with the generation of solid models representing lithological units and hydrothermal alteration domains. The modeling was based on both the original drillhole mining logs and updated data generated in this study, including core re-logging, and petrographic and spectroscopic analyses.

#### 4. Deposit geology

The mineralization observed in the drilling cores of the Santa Bárbara Deposit are hosted in both the lithotypes of the Passo do Feio Complex and the Camaquã Supergroup (Maricá and Bom Jardim Groups). The predominant lithotypes in the deposit include (i) quartz-feldspathic mica schists, carbonate-talc schists and amphibolites from the Passo do Feio Complex (Vacacaí Metamorphic Belt), associated with the Cerro dos Andradas shear zone; (ii) basalt dykes and andesites from the Bom Jardim Group; (iii) siltstones and sandstones from the Maricá Group; and (iv) fault cataclasites and mineralized hydrothermal breccias (Figure 2).

Figure 2: Simplified geological cross section A-B (see location in Figure 1), showing the main lithotypes found in the drill holes at the Santa Bárbara Deposit and the mineralization associated with the fault core and damage zones.

The host rocks for the mineralization associated with the shear zone that affect the Passo do Feio Complex primarily consist of intercalations of lithotypes, including quartz-chlorite schist, sericite-quartz schist, quartz-feldspar-biotite-chlorite schist, carbonate-chlorite-talc schist, and -amphibolites (Figures 3A to 3I). The mineralogy mainly includes subhedral plagioclase, anhedral recrystallized quartz, chlorite, biotite, and sericite, with variations between chloritic and biotitic varieties (Appendix 1A, 1B). Some sections contain talc and carbonate (Appendix 1C, 1D), intercalated with foliated rocks rich in actinolite, hornblende, and plagioclase (Appendix 1E, 1F). At deeper levels, porphyroblastic rocks with amphibole porphyroblasts indicate the presence of hornblende hornfels (cornubianites), as described by Leinz (1941). In the section related to the volcanic and subvolcanic rocks of the Bom Jardim Group, the rock exhibits a massive structure and fine holocrystalline equigranular texture, composed mainly of plagioclase, augite, chlorite, and magnetite.

Figure 3: Main lithotypes found in drill holes at the Santa Bárbara Deposit. (A) Chlorite-quartz schist (SB-02-337m); (B) Muscovite-chlorite-quartz schist (SB-02-516m); (C) Intercalation of actinolite amphibolite (dark level) and talc-chlorite schist (light level) (SB-02-593m); (D) Talc-carbonate schist (SB-02-585m); (E) Chloritized quartz-feldspathic mylonite (SB-03-72m); (F) Chloritized quartz-feldspathic cataclasite (SB-09-31m). (G) Andesitic basalt with carbonate-alteration halo in core SB-08 (120m); (H) Chloritized quartz-

feldspathic mylonite (SB-03-60m). (I) Chloritized quartz-feldspathic cataclasite (SB-09-69m).

The structures and textures associated with the deformation of the Andradas Fault are divided into fault core rocks (ultracataclasites and cataclasites) and the fault damage zone (protocataclasites, stockwork fractures, and hydrothermal breccias). This brittle deformation affects both the mylonitic lithologies of the Passo Feio and the sedimentary and volcanic rocks of the Camaquã Supergroup. Eastward from the fault damage zone, mylonite, phyllonite, and ultramylonite textures predominate in the Cerro dos Andradas Shear Zone, parallel to the mylonitic foliation of the western edge of the Caçapava do Sul Granite.

The main mineralized zone is primarily copper-rich and occurs within the damage zone of the Andradas Fault, oriented NNE-SSW, hosted in mylonitic quartz-chlorite schists and brecciated andesites (Figures 4A and 4B). The copper ore mainly consists of hydrothermal breccias with a quartz-carbonate composition, chalcopyrite sulfide-bearing, featuring stockwork vein structures and cataclastic texture (Figures 4C and 4D).

From the Andradas Fault, located between boreholes SB-03 and SB-06 (UTM E 258200 x UTM N 6631900), the copper zone is estimated to extend about 400 meters west, 100 meters east, 500 meters southwest, and 700 meters northeast. This delineates a tabular body measuring about 500m by 1200m within the fault damage zone, indicating a shallow body in a brittle deformation environment.

At depth, the mineralized cataclastic deformation zone extends down to -300 meters and follows the estimated fault trace to -600 meters to the west. This is evidenced by borehole SB-04, which intersects the cataclastic zone at about 600 meters and shows mineralization in that section.

In another part of the deposit, located 1,000 meters east of the Andradas Fault at -550 meters, copper mineralization is hosted in amphibolites and chlorite-talc schists (Figure 4E). While associated with areas of higher deformation, the mineralization appears as hydrothermal breccia similar to that linked with the damage zone of the Andradas Fault, composed of sulfide-bearing quartz-carbonate with chalcopyrite (Figure 4F). This sector also contains zinc and lead mineralization associated with sulfide-bearing carbonate veins and veinlets, with sphalerite and galena (Figure 4G), as well as disseminated sulfides within the mylonitic foliation (Figure 4H).

Figure 4: Detail of copper occurrences at the Santa Bárbara Deposit intercepted by drill holes. (A) Calcitic and Fe-dolomitic hydraulic breccia with fragments of argillized chlorite-quartz schist in core SB-09 (52m-); (B) Brecciated andesitic basalt with sulfide-bearing carbonate veins in core SB-08 (121m); (C) Sulfide-bearing calcitic and Fe-dolomitic with chalcopyrite vein cutting argillized chlorite-quartz schist in core SB-06 (161m); (D) Stockwork-style vein of sulfide-bearing carbonate composition with chalcopyrite cutting cataclastic and mylonitic chlorite schist quartz-feldspathic in core SB-03 (65m); (E) Fe-dolomitic and calcitic hydraulic breccia with fragments of chlorite-quartz schist (640m); (F) Sulfide-bearing Fe-dolomitic and calcitic hydraulic breccia with chalcopyrite within fragments of amphibolite (655m); (G) Sulfide-bearing carbonate vein with sphalerite and galena (644m); (H) Sericite-chlorite schist with concordant sphalerite



and galena mineralization along mylonitic foliation (711m).

Zn-Pb mineralization occurs in veins similar to those mineralized with copper, indicating a contemporaneous mineralizing event for all base metals. Furthermore, anomalous levels of As, Au, Mo, Sn, and W accompany the Zn-Pb anomalies, suggesting a polymetallic source for the mineralizing fluids. Table 2 shows the anomalous levels for As, Ag, Au, Cu, Mo, Pb, Sn, W and Zn. The maximum copper levels occur in the 640m sections of SB-02 (6,662 ppm), 57m of SB-03 (5,650 ppm), 74m of SB-05 (1,000ppm), 161m of SB-06 (5,220 ppm), 264m of SB-07 (3,070 ppm), 139m of SB-08 (8,890 ppm) and 39m of SB-09 (3,790 ppm). The maximum levels of the other anomalous metals occurred only in borehole SB-02, at the following depths: 707m (6,544 ppm in Zn and 3,186 ppm in Pb), 708m (2134 ppm in As), 771m (1842 ppm in Au). To a lesser extent, but anomalously, there are concentrations of Ag (748 ppm), Sn (281 ppm) Mo (151 ppm) and W (116 ppm). Table 2 presents the anomalous concentrations for As, Ag, Au, Cu, Mo, Pb, Sn, W, and Zn. The highest copper levels are found at the following depths: 640m in SB-02 (6,662 ppm), 57m in SB-03 (5,650 ppm), 74m in SB-05 (1,000 ppm), 161m in SB-06 (5,220 ppm), 264m in SB-07 (3,070 ppm), 139m in SB-08 (8,890 ppm), and 39m in SB-09 (3,790 ppm). The maximum concentrations of other anomalous metals are only in borehole SB-02 at these depths: 707m (6,544 ppm Zn and 3,186 ppm Pb), 708m (2,134 ppm As), and 771m (1,842 ppm Au). Additionally, there are lower but still anomalous concentrations of Ag (748 ppm), Sn (281 ppm), Mo (151 ppm), and W (116 ppm).

Table 2: Geochemical results for nine anomalous metals at the Santa Bárbara deposit. The sections were sampled by the mineral prospecting company and analyzed by the Intertek laboratory. Source: Mining Ventures and Intertek reports. Abbreviations: NA: not analyzed; LD: Detection limit.

## 5. Hydrothermal alteration

The host rocks of the Santa Bárbara deposit are intensely affected by hydrothermal alteration, exhibiting textural patterns typical of overprinting processes. The hydrothermal mineral assemblages observed indicate the occurrence of chloritization, epidotization, albitization, potassification, sericitization, carbonatization, argillization and silicification processes, in both fissure and pervasive styles. Results of macro- and microscopic descriptions, as well as VNIR-SWIR spectroscopy results are presented. These analyses were carried out on representative drill core samples from the deposit, which supported the characterization of the main types of hydrothermal alteration observed.

### 5.1. Carbonatization

The carbonate alteration is the main hydrothermal process associated with the ore minerals in the Santa Bárbara deposit. Although it occurs in purely carbonate compositions and can also be associated with post-mineralization processes, this alteration is closely related with sulfidation, silicification and sulfation processes. The carbonatization occurs in both pervasive and fissure styles, in the form of white to yellowish-white hydrothermal veins and breccias, occasionally to grayish

or pinkish tones. The fissure style occurs as stockworks of veinlets and veins, with millimeter- to centimeter- dimensions. Pervasive alteration occurs in the form of metric to decametric carbonate hydrothermal breccias with associated alteration halos, both in disseminated form and in concentrated veinlets. The veins and breccias have a cataclastic and stockwork structure and a banded, colloform and syntaxial texture (Figures 5A to 5F). They are composed of calcite, Fe-dolomite, quartz, gypsum, barite, chalcopryite, sphalerite and galena (Appendix 2A to 2I). The carbonate, quartz and gypsum crystals that fill the veins are generally euhedral, with the presence of hexagonal quartz (Appendix 2C), prismatic gypsum (Appendix 2H, 2I) and fine- to coarse-grained tabular barite. Fine- to medium-grained calcite and quartz can also be found in subhedral to anhedral aggregates (Appendix 2A to 2C). Some carbonate veins occur in paragenesis with chlorite, epidote and hematite.

Figure 5: Carbonatization affecting the lithotypes at the Santa Bárbara Deposit and spectra of the lithological features. Arrows highlight the main absorption features, indicating the wavelength position, associated molecules/ions, and mineral interpretation. (A) Fe-carbonate vein with disseminated copper sulfides, colloform texture, and argillization halo, hosted in andesite (SB-08-117m-1916sp); (B) Sulfide-bearing calcitic and Fe-dolomitic with chalcopryite vein cutting argillized chlorite-quartz schist in core SB-06 (161m-2068sp); (C) Sulfide-bearing Fe-dolomitic and calcitic hydraulic breccia with chalcopryite within fragments of amphibolite (655m-1573sp); (D) Brecciated andesitic basalt with sulfide-bearing carbonate veins in core SB-08 (121m-1911sp); (E) Stockwork-style carbonate veining hosted in amphibolite (SB-02-619m-1606sp) within a lithochemical anomaly (Cu: 500ppm); (F) Sulfide-bearing carbonate vein with sphalerite and galena (644m-1567sp); . Abbreviations: cb: carbonate; chl: chlorite; Fe-cb: Fe-carbonate; il: illite; inclus.: water-bearing fluid inclusion; sp = spectral analysis number.

Sulfides are found mainly associated with the carbonatization of halos. There is a predominance of fine- to coarse-grained chalcopryite with anhedral granular habit. These crystals exhibit lamellae and edges of bornite exsolution (Appendix 2F), as well as quartz and gypsum inclusions, in association with covellite and pyrite (Appendix 2G). Some chalcopryite crystals have irregular, lobed edges, which indicate a late, post-carbonatization development. Some veins show euhedral sphalerite and galena, associated with few or no copper sulfide (Appendix 2D, 2E).

There is also a post-mineralization carbonate phase composed of millimetric calcite veins with associated chlorite. Some of these veins show evidence of late brittle deformation, such as incipient undulating extinction in the quartz, and microgranular recrystallization of quartz and barite, with deformation twinning.

Spectral signatures taken from the carbonate alteration (Figures 5A to 5F) are dominated by the typical  $\text{CO}_3^{2-}$ -related absorptions, with deep and asymmetrical features at ~2325 to ~2340 nm (Gaffey, 1986). The variation in the wavelength position of this feature, together with the presence or absence of secondary  $\text{Fe}^{2+}$ -related features at ~1060 and ~1270 nm, indicated the occurrence of Fe-dolomite and calcite in the analyzed samples (Figures 5A to 5F). The Fe-dolomite spectra

are the most abundant of them, occurring predominantly in the veinlets and veins associated with the mineralized zones, whereas the calcite spectra occur essentially in the barren zones.

## 5.2. Argillization

Argillization is also a significant hydrothermal process related to the mineralized zones. The mineral characterization of this type of alteration was carried out mainly using the systematic VNIR-SWIR spectroscopic survey and the macroscopic descriptions (Figures 6A to 6F and 7A to 7F) of the drill core samples. The key minerals described in the argillic zones make up a mixture of illite, smectite and sericite. Macroscopically, these minerals occur in pervasive and fissural styles, with yellow-orange and light grey colors, very fine granulation and xenomorphic texture. Although it is difficult to be distinguished under optical microscopy due to its very fine granulometry, illite was described in thin sections (Appendix 1M to 1R) as a filling mineral in the matrix of ultracataclastic zones in the hydrothermal breccias, associated with sericite levels.

Figure 6: Argillization affecting the lithotypes at the Santa Bárbara Deposit and spectra of the lithological features. Arrows highlight the main absorption features, indicating the wavelength position, associated molecules/ions, and mineral interpretations. (A) Reddish fissural argillization cut by carbonate veining (SB-06-141m-2098sp); (B) Beige fissural argillization cut by chalcopryite veins (SB-06-150m-2088sp); (C) Pervasive argillization with associated sericite, intersected by carbonate veining (SB-08-124m-1907sp); (D) Pervasive argillization parallel to mylonitic foliation (SB-06-55m-2211sp); (E) Carbonate vein with a illite-sericite alteration halo (SB-06-155m-2079sp); (F) Fissural argillization affecting both chloritized (green) and albitized (pink) portions (SB-06-87m-2167sp); Abbreviations: cb: carbonate; chl: chlorite; il: illite; inclus.: water-bearing fluid inclusion; sp: spectral analysis number.

Figure 7: Argillization affecting the lithotypes at the Santa Bárbara Deposit and spectra of the lithological features. Arrows highlight the main absorption features, indicating the wavelength position, associated molecules/ions, and mineral interpretations. (A) Hydrothermal breccia with clay matrix and fragments of albitized and potassic rock (SB-09-53m-2003sp); (B) Fissural-pervasive argillization associated with a sulfide zone (SB-06-94m-2159sp); (C) Carbonate vein with a argillization halo (SB-06-57m-2208sp); (D) Generalized pervasive argillization associated with a carbonate vein (SB-06-65m-2199sp); (E) Fissural argillization in a silicified zone (SB-08-124m-1908sp); (F) Sulfide vein with associated silicification and gray argillization (SB-09-58m-1949sp). Abbreviations: cb: carbonate; chl: chlorite; il: illite; inclus.: water-bearing fluid inclusion; sp: spectral analysis number.

Spectroscopically, white micas (sericite or muscovite) and illites have very similar signatures (AIOH features at ~2200, ~2350 and ~2450 nm, H<sub>2</sub>O features at ~1910 nm, and OH features at ~1410 nm) (Hunt & Salisbury, 1970) (Figures 6 and 7), and they are easily distinguished by differences in the intensity of the H<sub>2</sub>O-related absorption (weak for white

micas and strong for illite). However, when these minerals occur in spectral mixtures with overlapping free water absorption features (Figures 6 and 7) the identification may be ambiguous, which makes it difficult to separate the argillic and sericite events.

Although the petrographic results suggest the association of sericite and illite in the same hydrothermal event, VNIR-SWIR spectroscopy defined that the occurrence of spectral signatures dominated by illite-sericite features represented the argillic phase, whereas those dominated by sericite-muscovite features represented the sericite phase. This interpretation is also supported by the occurrence of pure spectra of illite associated with sulfide-bearing, silicified carbonate veins (Figure 7F), representing a mineralizing phase devoid of the lamellar muscovite crystals identified in the macroscopic analyses, which would be related with a sericitization phase before to the argillization. Therefore, it is understood that the argillic alteration represents the proximal hydrothermal zone to the mineralized bodies, being characterized by the occurrence of illite as the main mineral phase. Accordingly, there are at least three events related to the sericite-illite mineral phases: (i) sericitic event, pervasive-selective, before to the pure illitic event; (ii) pervasive illitic-sericitic event, prior and proximal to the mineralized veins; and (iii) fissural pure illitic event, in which illite occurs in paragenesis with carbonates, quartz and copper sulfides.

The crystallinity variation in the sericite-illite-smectite series (Pontual et al., 2008) was investigated through the analysis of the ratio between the AIOH absorption at ~2200 nm and the H<sub>2</sub>O absorption at ~1910 nm in a suitable set of spectral signatures. The obtained values were compared with the varying concentrations of Cu (ppm) observed in drill core samples. The results (Figure 8A) demonstrate a broad range of crystallinity for this mineral series at concentrations up to 300 ppm, likely influenced by the different sampled lithologies. At concentrations exceeding 300 ppm, a decreasing trend in crystallinity is observed with increasing Cu levels, characterized by a predominance of illite and illite-smectite for concentrations between 300 and 1000 ppm, and smectite-illite for concentrations above 1000 ppm.

Similarly, variations in the wavelength position of the AIOH absorption at ~2200 nm (~2185 to ~2225 nm) in illite-sericite spectral signatures are related to compositional differences in these minerals, indicating abundance in Na, K, or Fe-Mg (Pontual et al., 2008). The analysis of this spectral feature along representative drill core sections, compared with the Cu concentrations (ppm) (Figure 8B), indicates a predominantly potassic composition for the argillic event, with a subtle trend towards an iron-magnesium composition at concentrations above 2000 ppm of Cu.

## 5.3. Chloritization

Chloritization has a broad distribution in the core samples. It occurs in pervasive, selective-pervasive, and fissural styles, and affects most host lithotypes of mineralization. Its main diagnostic characteristic is the green to dark gray color of cataclastic and mylonitic rocks (Figures 9A to 9F). In thin sections, it occurs as anhedral, lamellar, or tabular crystals, ranging from fine to very fine grain size, and along cataclastic and mylonitic structures (Appendix 1G to 1L). In cataclasites, chlorite occurs pervasively, as a fracture-filling

mineral in brecciated quartz-feldspar fragments (Appendix 1G). In mylonites, it occurs pervasively in schistosity bands, replacing mafic minerals and associated with other phyllosilicates such as muscovite, biotite, or talc (Appendix 1H). In andesites, this alteration occurs in selective-pervasive and fissural styles, altering mafic minerals and occupying the interstices of saussuritized plagioclase crystals (Appendix 1I). Associated with mineralized veins, hydrothermal chlorite occurs in fissural style in at least two temporal phases: (i) contemporaneous with carbonatic veins containing quartz and sulfides, occurring at the edges of these veins (Appendix 1J, 1K); and (ii) late-stage, associated with sericite or illite veins and veinlets (Appendix 1L).

Chlorite spectral signatures are defined by FeOH and MgOH absorptions at ~2250 and ~2350 nm, respectively (Clark et al., 1990) (Figure 9). Variations in the wavelength positions of these features indicate differing Fe and Mg contents in chlorite (Pontual et al., 2008). Secondary chlorite features at ~750, ~930, and ~1130 nm (Fe<sup>2+</sup>), ~1410 nm (OH), and ~2000 nm (H<sub>2</sub>O) (Clark et al., 1990; Pontual et al., 2008) (Figure 9) are also crucial for identification, particularly in spectral mixtures with other minerals that have overlapping diagnostic features (e.g., biotite, epidote, amphiboles, and carbonates).

In the analyzed samples, diagnostic chlorite features are abundant across all sections, characterizing both the mineralogy of unaltered rocks (dynamic and contact metamorphism) and various hydrothermal alteration horizons and mineralized zones. Compositional variations in chlorite were assessed by analyzing the position of the FeOH feature at ~2250 nm and comparing it to Cu concentrations (ppm) in the drill core samples (Figure 8C). This investigation aimed to evaluate potential compositional distinctions between chlorites of metamorphic and hydrothermal origin and/or to identify compositional vectors toward proximal ore zones. Results indicate a predominantly lithological control, with no compositional trend related to the ore. Fe chlorites, Mg-chlorites, and intermediate (FeMg-chlorites) compositions occur both below 300 ppm and above 1000 ppm (Figure 8C).

Figure 8: (A) Graph showing the variation in crystallinity of the sericite-illite-smectite series based on the ratio between the depths of absorption features related to AlOH and H<sub>2</sub>O, about the Cu concentration (ppm) in the drill cores of the Santa Bárbara Deposit; (B) Graph showing the compositional variation of illite-sericite based on the wavelength position of AlOH absorption, about the Cu concentrations (ppm) in the drill cores of the Santa Bárbara Deposit; (C) Graph showing the compositional variation of chlorites based on the wavelength position of FeOH absorption, about the Cu concentrations (ppm) in the drill cores of the Santa Bárbara Deposit.

Figure 9: Chloritization affecting the lithotypes at the Santa Bárbara Deposit and spectra of the lithological features. Arrows highlight the main absorption features, indicating the wavelength position, associated molecules/ions, and mineral interpretations. (A) Pervasive alteration in mylonitic quartz-chlorite schist (SB-06-70m-21871sp); (B) Pervasive alteration in mylonitic quartz-chlorite schist (SB-02-443m-1812sp); (C) Selective pervasive alteration in mylonitic muscovite-biotite quartz-feldspathic schist (SB-02-778m-1371sp); (D) Selective pervasive alteration in talc schist and banded mylonitic

amphibolite (SB-02-579m-1653sp); (E) Fissural alteration associated with carbonate veins, cutting through mylonitic quartz-chlorite schist and amphibolite (SB-02-517m-1727sp); (F) Fissural alteration associated with carbonate veins cutting through amphibolite (SB-02-614m-1612sp). Abbreviations: bt: biotite; cb: carbonate; chl: chlorite; Mg-chl: Mg-chlorite; tlc: talc; sp: spectral analysis number.

#### 5.4. Sericitization

Sericitization occurs with restricted distribution, primarily altering the feldspars of chloritized quartz-feldspar mylonites, in selective-pervasive and fissural styles (Figures 10A to 10D). Also known as phyllic alteration, it typically consists of fine sericite grains aligned with the mylonitic foliation (Appendix 2J), but can develop into visible muscovite crystals (Appendix 2K). Although associated with chloritization, hydrothermal sericite is temporally linked to an earlier phase of chloritization, evident in some cataclasites and hydrothermal breccias containing sericitized rock fragments (Appendix 2L). Post-mineralization, sericite appears in veinlets alongside chlorite and quartz. Subordinate hydrothermal sericite is also associated with pervasive argillization and sulfide-bearing carbonatic veins, though not recognized as a significant phase related to mineralization. These domains of pervasive argillization with subordinate sericitization also exhibit pervasive carbonatization, appearing as anhedral masses or corroded grains, likely indicating destabilization of this mineral phase.

Figure 10: Sericitization affecting the lithotypes at the Santa Bárbara Deposit and spectra of lithological features. Arrows highlight the main absorption features, indicating the wavelength position, associated molecules/ions, and mineral interpretations. (A) Chloritized and sericitized quartz-feldspathic mylonite (SB-08-138m-1893sp); (B) albitized and sericitized chlorite quartz-feldspar schist, (SB-09-58m-2004sp); (D) Selective pervasive alteration in mylonitic quartz-chlorite schist (SB-02-631m-1581sp); (C) Pervasive alteration in chlorite quartz-feldspathic schist, albitized and sericitized, intersected by carbonate veinlets (SB-09-70m-1991sp). Abbreviations: bt: biotite; chl: chlorite; inclus.: water-bearing fluid inclusion; ser: sericite; sp: spectral analysis number.

Spectral signatures of sericite (white micas) are characterized by AlOH absorptions at ~2200, ~2350, and ~2450 nm, associated with OH absorption at ~1410 nm and a weak to absent H<sub>2</sub>O absorption at ~1900 nm (e.g., Hunt & Salisbury, 1970). In the analyzed samples, sericite-related features are observed in restricted spectral mixtures, primarily with chlorite, but also with quartz and biotite (Figure 10), occurring in non-hydrothermally altered schists and mylonites and distal zones of pervasive alteration. Compositional variations in sericite were not assessed due to the low number of spectral features identified for this mineral.

#### 5.5. Potassification

Potassic alteration was observed only in short segments (up to 15 meters in linear thickness) of the drill cores SB-07, SB-08, and SB-09 (Figure 11). This alteration is characterized by the replacement of igneous feldspars by hydrothermal



K-feldspar, which imparts a reddish color and a cloudy, “dirty” appearance to the pseudomorphous igneous crystals (Appendix 2P). It occurs predominantly in a pervasive style, affecting both quartz-feldspar tectonic breccias (Appendix 2Q, 2R) and subvolcanic andesitic rocks.

Figure 11: Core section from drill-hole SB-09 at the Santa Bárbara Deposit, Between Depths of 45m and 65m (Left to Right). This section shows pervasive potassic and albitic alteration (red and pink colors), overlaid by carbonate fissure zones (white) and illite-rich areas (beige), along with pervasive chloritization (dark gray). Abbreviations: fk+ab: feldspar and albite alteration; ilt+cb: illite and carbonate alteration; cb+sulf: sulfide-bearing carbonate alteration

Although its occurrence is spatially associated with carbonate and argillic alteration zones, potassic alteration is temporally linked to the early hydrothermal phases, contemporaneous with albitization processes, which will be described next. The analysis of the cross-cutting relationships between the different hydrothermal stages reveals the overlap of the potassic event with other types of alteration, such as chloritization, argillization, and carbonatization (Appendix 2Q).

## 5.6. Albitization

Albitization is a much localized alteration that is observed in small fragments of tectonic breccias, associated with the potassic alteration (Figure 11). Macroscopically, it is diagnosed by a light pink color (though microscopic analysis is required for confirmation). Hydrothermal albite (Appendix 2M to 2O) occurs in anhedral or tabular aggregates with fine to medium grain size, exhibiting anomalous polysynthetic and chessboard-type twinning. Typically, the albitized zones are intensely fragmented and are overlapped by other types of hydrothermal alteration, primarily the carbonatization. Similar to potassification, hydrothermal albite is temporally linked to the early phases of hydrothermal alteration, possibly representing the first hydrothermal process in the evolution of the fluid responsible for the polymetallic mineralization of the Santa Bárbara deposit.

## 5.7. Minor alterations

Other types of hydrothermal alteration, such as hematization, epidotization and skarnitization (hornblende skarn and talc skarn) are also observed in some sections of the drill core samples from the Santa Bárbara deposit (Figures 12A to 12D). However, it was not possible to establish temporal and spatial relationships between these processes and the mineralizing event, except for the skarnitization, which occurs before mineralization and is associated with lenses of metabasic and meta-ultrabasic rocks near the contact zone with the Caçapava do Sul Granite (bottom sections of drill hole SB-02). In this zone, hornblende porphyroblasts characterize hornblende hornfels (Figure 12A), which are associated with greenish-white veins and halos (Figure 12B) predominantly composed of epidote, occasionally accompanied by gypsum and zeolite.

Figure 12: Minor alteration types affecting the host rocks of the Santa Bárbara deposit and spectra of lithological features.

Arrows highlight the main absorption features, indicating the wavelength position, associated molecules/ions, and mineral interpretations. (A) hornfels with hornblende porphyroblasts and greenish epidote alteration halo (SB-02-872m-1227sp); (B) epidote-rich veins with gypsum and zeolite hosted in amphibolites (SB-02-933m-1138sp); (D) reddish hematite-goethite alteration veins associated with the green clay zone (SB-06-47m-2224sp); (C) reddish hematite-goethite-rich vein with brecciated and stockwork textures (SB-06-28m-2253sp). Abbreviations: cb: carbonate; chl: chlorite; dol: dolomite; ep: epidote; gp: gypsum; hbl: hornblende; hem: hematite; inclus.: water-bearing fluid inclusion; ser: sericite; tlc: talc; zeo: zeolite; sp: spectral analysis number.

The mineralogical characterization of these type of hydrothermal alterations was done primarily through macroscopic descriptions enhanced by VNIR-SWIR spectroscopic interpretations (Figure 12). Epidote was identified by OH absorptions at ~1545 and ~1830 nm (Roache et al., 2011), as its more prominent spectral features (~2255 and ~2340 nm) may be overlapped in spectral mixtures with amphibole, biotite, chlorite, or carbonates (Figure 12). Zeolite spectral signatures are characterized by deep, asymmetrical absorptions at ~1430 and ~1920 nm (e.g., Cloutis et al., 2002) (Figure 12). Gypsum is identified by the typical H<sub>2</sub>O absorptions at ~1500 and ~1940 nm, as well as the OH absorption at ~1750 nm (Pontual et al., 2008) (Figure 12).

Hornblende and actinolite exhibit similar VNIR-SWIR spectral signatures, with diagnostic MgOH absorptions at ~2325 and ~2315 nm, and secondary features centered at ~2390 and ~2380 nm, respectively (Pontual et al., 2008). However, actinolite can be distinguished by a sharp OH absorption at ~1400 nm, which is absent in the hornblende spectra (Clark et al., 1990). These minerals occur as porphyroblasts in the hornfels, as well as primary minerals in the metabasic rocks. Talc spectral signatures are characterized by diagnostic MgOH absorptions at ~2310 and ~2290 nm, with secondary features at ~2390 nm and OH absorption at ~1395 nm (Pontual et al., 2008).

## 6. Discussion

The mineralization of the Santa Bárbara deposit are hosted in a hydrothermalized ductile-brittle shear zone oriented NNE-SSW, geologically and structurally continuous with the Cerro dos Andradas fault-related ore occurrences and lithotypes to the south. The ductile phase is associated with the synkinematic intrusion of the Caçapava do Sul granite, marking the onset of its exhumation and the development of deformation of the granite and its metavolcano-sedimentary host rocks. Conversely, the brittle phase is related to the nucleation of a master fault of the Camaquã Rift and the evolution of the Western sub-basin (Andradas or Santa Bárbara Fault), which controls the exposure and denudation of the Caçapava do Sul High as well as the generation of cataclasis on the schists and mylonites of “Passo Feio Complex and andesites of the Hilário Formation.

The brittle structures and textures in the Andradas Fault zone were classified into a fault core composed of ultracataclasites and cataclasites, and a damage zone comprising protocataclasites, veins, and hydrothermal breccias. Copper anomalies concentrate in the structures



of the damage zone, indicating that the structural control of the mineralized bodies is closely associated with the brittle deformation of the master fault of the Camaquã Rift (Andradas Fault). Faults of this type are associated with kilometer-scale displacements that accommodate movement between the blocks and control the mechanical subsidence of the basin. The estimated thickness of the Andradas Fault damage zone is approximately 300 meters. To the south of the studied area, this fault trends from N-S to NE-SW, configuring a curved geometry on the field. Similar examples include epithermal, skarns, and porphyries deposits from the Colorado Mineral Province, which were formed during crustal extension associated with the formation of the Rio Grande Rift (Basin and Range). These deposits are spatially related to tectonically active zones that control faults and regional lineaments (Kelley et al., 2020; Chapin, 2012). Since the definition of the "Sul-Riograndense Copper Polygon", Ribeiro et al. (1966) proposed a key structural control for copper mineralization, associated with the major fault zones, primarily oriented NE-SW. Additionally, it is noted that the migration of mineralizing hydrothermal fluids is favored by a syn-tectonic development of extensional faults, and cataclastic and dilatational zones related to the exhumation of the Caçapava do Sul granite pluton. Due to their high permeability and porosity, these brittle structures indicate zones of fluid transport and deposition. Therefore, it is assumed that the Andradas Fault comprises the main structural element that conditions the migration and deposition of the ores at the related fault deposits.

Ribeiro et al. (1966) described the andesitic volcanism (Crespos Formation, later renamed the Hilário Formation) as the magmatic source of copper, asserting that the only occurrences unrelated to the andesites would be from Cerro dos Andradas (Santa Bárbara, Andradas, and Primavera deposits). However, this study indicates that the undeformed andesitic and basaltic dikes, possibly related to the volcanic event of the Hilário Formation, have been affected by the mineralizing hydrothermal event. Therefore, the mineralization of the Santa Bárbara deposit are not exclusively associated with the metamorphic basement.

The metamorphism of the Cerro dos Andradas fault zone rocks is predominantly dynamic and conditioned by the interaction of magmatic fluids from the Caçapava do Sul granite with its host rocks. This study identifies at least two metamorphic phases: skarnitic (related to the contact metamorphism) and hydrothermal (related to a later event). Skarnitization is interpreted as a pre-mineralization phase occurring in a high-temperature ductile deformation environment, resulting from the intrusion of the adjacent granite pluton into the basement rocks. This event generates the amphibole hornfels (cornubianites) at the granite's margin and alters the mineral compositions in lenses of metaultrabasic rocks (magnetite-rich chloritites and chromiferous serpentinites) and magnesian calc-silicates (carbonate-talc schists).

In the shear zone, frequent lithological intercalations parallel to the mylonitic foliation reflect not only variations in the protolith composition but also differing intensities of deformation and hydrothermal alteration. No intrusive or discordant contacts are observed between the granite and schists, as all lithotypes are affected by mylonitic deformation. Thus, variations of mylonitic quartz-feldspathic mica schists, quartz-chlorite phyllonites, and albite-chlorite schists may result from the shearing and hydrothermal alteration of granitic

protoliths. Field relationships, along with the ages reported in the literature (Remus et al., 2000a; Battisti et al., 2023), suggest a temporal overlap between granite intrusion, deformation, and the protoliths that were later mylonitized. This scenario supports the previously mentioned hypothesis. On the other hand, serpentine-talc-chlorite schists, calc-silicates would be products of deformation and contact metamorphism of the host rocks (dolomite and metaultrabasic). The mineralogy of these rocks is consistent with undeformed magnesian skarns described at the eastern margin of the Caçapava Granite (Hoerlle et al., 2023), which may indicate the presence of a skarn system in the deposit area. However, petrochronological and geochemical analyses would be necessary to test this idea.

Hydrothermal alteration is the major geological process identified as conditioning the generation of polymetallic mineralization in the Santa Bárbara deposit.

This study supported the preliminary identification of key minerals (Table 3) related to potential hydrothermal zoning (distal and proximal) about the mineralized zones (sulfidation with sulfation, silicification and carbonatization). Distal zones are characterized by pervasive chloritization, while proximal zones exhibit fissural potassic alteration and argillization, as shown in Figures 13A and 13B. The abundant presence of chlorite in the Passo do Feio metamorphites near Cerro dos Andradas has been associated with low-grade regional metamorphism of mafic/intermediate rocks (metavolcanics). In this context, Ribeiro et al. (1966) and Ribeiro (1978) associated the metamorphic rocks adjacent to the granite with the green schists of the basement unit (Vacacaí Formation/Subgroup).

Figure 13: Model of alteration zones of the Santa Bárbara deposit. (A) 3D hydrothermal model showing epithermal carbonation stockwork vein system and argillization halo; (B) 2D hydrothermal model superposed on geological profile showed in Figure 2.

Chlorite associated with copper mineralization, as products of skarnitization and epithermal systems, has been documented in other occurrences within the Camaquã Basin and in the vicinities of the Caçapava do Sul granite (Troian, 2009; Reis et al., 2017; Hoerlle et al., 2023). In the Uruguai copper mine, in the Minas do Camaquã region, chlorite comprises one of the main hydrothermal minerals. Troian (2009) describes three generations of chlorite, occurring both pervasively, impregnating the sandstone framework, and associated with mineralized veins and fractures. The formation of endoskarns through chloritization of the Caçapava do Sul granite is described as a product of metasomatism of the dolomitic host rock (Reis et al., 2017; Hoerlle et al., 2023).

In this study, chloritization is considered one of the main hydrothermal processes, occurring in pervasive style in the altered host rocks, and fissural style in the hydrothermal breccias and mineralized veins. Considering the occurrences described in previous studies, as well as the context of a syn-magmatic shear zone, the hypothesis of an essentially hydrothermal origin for the chlorites in the Cerro dos Andradas fault zone rocks is considered valid. However, other studies (e.g., Remus et al., 2000a) interpret the chlorite in the mylonitic foliation as a product of regional metamorphism of the basement. The abundant presence of chlorite in the Passo do Feio metamorphites near Cerro dos Andradas has been

associated with low-grade regional metamorphism of mafic/intermediate rocks (metavolcanics). In this context, Ribeiro et al. (1966) and Ribeiro (1978) associated the metamorphic rocks adjacent to the granite with the green schists of the basement unit (Vacacaí Formation/Subgroup). Petrochronological and geochemical mineral analyses could provide valuable insights into this issue.

Albitic and potassic alterations are the result of high-temperature fluid circulation and represent the earliest set of hydrothermal alteration processes affecting the rocks in the deposit area. These alteration phases are observed in a restricted areas and were likely overprinted by later events of chloritization, argillization, and carbonation.

Carbonation represents the main hydrothermal mineralizing event, characterized by brecciation due to high fluid pressure, with open-space filling textures associated with brittle tectonics related to the activity of the master fault. During this phase, abundant veinlets and veins form a stockwork system, filled with ankerite, dolomite, quartz, gypsum, and barite, with associated chalcopyrite and bornite.

Furthermore, the presence of low-temperature hydrothermal clay minerals (illite and smectite) in proximal zones suggests that hydrothermal processes related to metal deposition occurred under shallow crustal conditions, possibly within an epithermal mineral system, which typically forms at depths of less than 1.5 km and temperatures below 300 °C (Sillitoe and Hedenquist, 2003; Simmons et al., 2005; Wang et al, 2019).

Table 3: Hydrothermal zoning and the respective minerals identified by petrography and spectroscopy in the Santa Bárbara Target drill cores.

7. Conclusion

The Santa Bárbara deposit is primarily copper-rich, featuring meter-scale sections with high metal concentrations (up to 0.9%), mainly associated with an iron-rich carbonatization (Fe-carbonate). It is also polymetallic, containing significant concentrations of Pb and Zn (up to 0.6% and 0.4%, respectively), as well as anomalous levels of noble metals such as Ag, Au, Mo, Sn, and W.

We highlight the relationship between the mineralization and the following geological features: 1) the intrusion of the Caçapava do Sul Granite, a plutonic counterpart of syn-rift magmatism; 2) the Cerro dos Andradas shear zone; 3) the nucleation of a master fault in the basin during the uplift and exhumation of a structural high; 4) the development of a brittle and shallow damage fault zone that allows for structural control of the mineralized bodies.

The results indicate that mineralized bodies are mainly sulfide-rich quartz-carbonate hydrothermal breccias, hosted in both: the metamorphic rocks of Passo do Feio Complex along the Cerro dos Andradas fault zone and the subvolcanic rocks of the Bom Jardim Group.

The presence of extensive gangue minerals (quartz, ankerite, gypsum, and barite), along with disseminated argillization halos surrounding the ore zones, and the metallogenic similarities between the Andradas and Primavera deposits suggest low-temperature hydrothermal processes (<300 °C) throughout the Cerro dos Andradas shear zone.

The association of diverse hydrothermal mineral

paragenesis with the polymetallic nature suggests that the mineralizing fluids primarily originate from magmatic hydrothermal sources, likely linked to the evolution of mid-Ediacaran syn-rift magmatism (around 560 Ma or earlier).

Finally, we propose that the base metal occurrences in the Cerro dos Andradas Shear Zone are associated with an epithermal mineral system related to the evolution of the Camaquã Basin, similar to other known deposits in the area.

Acknowledgements

This research was supported by the Geological Survey of Brazil (SGB-CPRM) under the project on the Geological and Metallogenic Evolution of the Cambrian-Ediacaran Volcano-sedimentary Basins in the Mantiqueira and Borborema Provinces. We thank to the researchers and technicians of the Rio Grande do Sul SGB-CPRM office for their support in the fieldwork and access to the drill cores, especially Alexandre Zanetti and Lucy Takehana. We also appreciate the valuable discussions with geologist Carlos Iglesias, Jorge Laux, Rafael Bittencourt, and Professors Drs Giuseppe de Toni, Vinicius Meira, Caetano Juliani, and Lena Monteiro, whose insights significantly enriched this work.

Authorship credits

Author	A	B	C	D	E	F
FEM						
BBT						
JLCN						
RGL						
GITG						

A - Study design/ Conceptualization    B - Investigation/ Data acquisition  
C - Data Interpretation/ Validation    D - Writing  
E - Review/Editing    F - Supervision/Project administration

References

Almeida D.P.M., Zeffass H., Basei M.A., Petry K., Gomes C.H. 2002. The Acampamento Velho Formation, a lower Cambrian bimodal volcanic package: geochemical and stratigraphic studies from the Cerro do Bugio, Perau and Serra de Santa Bárbara (Caçapava do Sul, Rio Grande do Sul, RS – Brazil). *Gondwana Research*, 5, 721-733.

Almeida D.P.M., Chemale Jr. F., Machado A. 2012. Late to post-orogenic Brasiliano-Pan-African volcano-sedimentary basins in the Dom Feliciano Belt, southernmost Brazil. In: Al-Juboury, A. I. (ed.). *Petrology: new perspectives and applications*: Rijeka, Croatia Intech, p. 73-130.

Almeida R.P., Janikian L., Fragoso Cesar A.R.S., Fambrini G.L. 2010. The Ediacaran to Cambrian Rift System of Southeastern South America: Tectonic Implications. *The Journal of Geology*, 118, 145–161.

Almeida R.P., Santos M.G.M., Fragoso Cesar A.R.S., Janikian, L., Fambrini G.L. 2012. Recurring extensional and strike-slip tectonics after the Neoproterozoic collisional events in the southern Mantiqueira province. *Anais da Academia Brasileira de Ciências*, 84, 347-376.

AGUIA Resources Limited; 2021. Andrade Copper Project; Caçapava do Sul; RS, Brasil Updated Resources Estimate and Scoping Study - Memorandum - March 9th, 2021 Sydney, Australia, Unpublished report. Available online at: <https://aguiaresources.com.au/asx-announcements/andrade-copper-updated-resource-estimate-scoping-study/> (accessed on 30 September 2024).

Badi W.S.R., Gonzalez A.P. 1988 Jazida de metais básicos de Santa Maria, Caçapava do Sul-RS. In: Schobbenhaus C., Silva C.E.C. (eds.). *Principais Depósitos Minerais do Brasil*, vol. 3, Rio de Janeiro , DNPM/ CVRD, p. 157-170.

Bettencourt J.S. 1972. A Mina de Cobre de Camaquã, Rio Grande do Sul. PhD Thesis, Instituto de Geociências, Universidade de São Paulo, São Paulo, 175 p.

- Battisti M.A., Bitencourt M.F., Nardi L.V.S., Florisbal, L.M., Slama J., Ackerman L., Padilha D.F. 2023. Unravelling major magmatic episodes from metamorphic sequences of the Dom Feliciano Belt central sector, Brazil – a comparative study of geochronology, elemental geochemistry, and Sr-Nd data. *Precambrian Research*, 385, 106951.
- Battisti M.A., Konopasek J., Bitencourt M.F., Slama J., Percival J.J., De Toni G.B., Carvalho da Silva S., Costa E.O., Trubac J. 2024. Petrochronology of the Dom Feliciano Belt foreland in southernmost Brazil reveals two distinct tectonometamorphic events in the western central Kaoko–Dom Feliciano–Gariép orogen. *International Journal of Earth Sciences*, 113, 973-1004.
- Bitencourt M.F. 1983. Metamorfitos da região de Caçapava do Sul, RS – Geologia e relações com o corpo granítico. In: *Simpósio Sul-Brasileiro de Geologia*, 1, 37–48.
- Brito L., Juliani C., Lago S. 2023. O Depósito de Santa Maria e as ocorrências de metais de base na Bacia do Camaquã. *Geologia USP Série Científica*, 23, 187-206.
- Bulhões C.S.A., Silva H.V.P., Pacheco G.S., Knak G.H., Fiore R.S., Strunkis V.T., Simões M.S., De Toni G.B. 2023. Detalhamento estrutural e petrográfico das mineralizações de cobre da Mina Primavera, Complexo Metamórfico Passo Feio, Caçapava do Sul-RS. In: *Simpósio Sul Brasileiro de Geologia*, 12, 79.
- Charles E. Chapin; Origin of the Colorado Mineral Belt. *Geosphere* 2012;; 8 (1): 28–43. doi: <https://doi.org/10.1130/GES00694.1>
- Clark R.N., King T.V.V., Klejwa M., Swayze, G.A. Vergo N. 1990. High spectral resolution reflectance spectroscopy of minerals. *Journal of Geophysical Research*, 95, 12653-12680.
- Clark R.N. 1999. Spectroscopy of rocks and minerals, and principles of spectroscopy. In: Rencz A.N. (ed.). *Remote sensing for the earth sciences: manual of remote sensing*. John Wiley and Sons. p.3-58.
- Cloutis E.A., Asher P.M., Mertzman S.A. 2002. Spectral reflectance properties of zeolites and remote sensing implications. *Journal of Geophysical Research*, 107, 1-19.
- Costa A.F.U., Fernandes L.A.D., Shukowsky W., Nardi L.V.S., Bitencourt M.F. 1995. Teste dos modelos tectônicos de posicionamento do Complexo Granítico de Caçapava do Sul através de estudos de modelagem gravimétrica 3-D. *Revista Brasileira de Geofísica*, 13, 91–101.
- De Toni G.B., Bitencourt M.F., Florisbal L.M., Martini A., Nardi L.V.S., 2024a. Anatomy of the transpressional Dom Feliciano Belt and its pre-collisional isotopic (Sr–Nd) signatures: a contribution towards an integrated model for the Brasiliano/PanAfrican orogenic cycle. *Gondwana Research*, 125, 180–209.
- De Toni G.B., Costa J.A.L. 2024b. Kinematic analysis of the Caçapava do Sul Granitic Complex, southern Brazil: Ediacaran syntectonic magmatism and strain partitioning during inclined ductile extrusion along a transpressional shear zone, Dom Feliciano Belt. *Journal of South American Earth Sciences*, 143, 104996.
- Fambrini G.L., Almeida R.P., Fragoso-Cesar A.R. 2006. Estratigrafia e evolução paleogeográfica do Grupo Santa Barbara (Eoediacarano) na Sub-bacia Camaquã Ocidental, Rio Grande do Sul, Brasil. *Revista Brasileira de Geociências*, 36, 550–565.
- Fernandes L.A.D., Tommasi A., Porcher C.C. 1992. Deformation patterns in the southern Brazilian branch of the Dom Feliciano belt: a reappraisal. *Journal of South America Earth Sciences*, 5, 77–96.
- Fontana E., Mexias A.S., Renac C., Nardi L.V.S., Lopes R.W., Barats A., Gomes M.E.B. 2017. Hydrothermal alteration of volcanic rocks in Seival Mine Cu–mineralization, Camaquã Basin, Brazil: part 1, chloritization process and geochemical dispersion in alteration halos. *Journal of Geochemical Exploration*, 177, 45-60.
- Fontana E., Renac C., Mexias A.S., Barats A., Gerbed M. C., Lopes R.W., Nardi L.V. S. 2019. Mass balance and origin of fluids associated to smectite and chlorite/ smectite alteration in Seival Mine Cu–Mineralization – Camaquã Basin –Brazil (Part II). *Journal of Geochemical Exploration*, Amsterdam, v. 196, 2019, p. 20–32.
- Fragoso-Cesar A.R.S., Fambrini G.L., Almeida R.P., Pelosi A.P.M.R., Janikian L., Riccomini C., Machado R., Nogueira A.C.R., Saes G.S. 2000. The Camaquã extensional basin: Neoproterozoic to Early Cambrian sequences in southernmost Brazil. *Revista Brasileira de Geociências*, 30, 442–445.
- Gaffey S.F. 1986. Spectral reflectance of carbonate minerals in the visible and near infrared (0.35–2.55 microns): calcite, aragonite, and dolomite. *American Mineralogist*, 71, 151–162.
- Hoerle G.S., Remus M.V.D., Müller T., Piazzolo S., Lana C., Sorger D. 2023. Metasomatic reactions triggered by localized and dynamically evolving fluid flux multistage intrusion history: an example from the syntectonic Caçapava do Sul Granitic Complex, Southern Brazil. *Lithos*, 442–443, 107103.
- Hunt G.R., Salisbury J.W. 1970. Visible and near-infrared spectra of minerals and rocks: I Silicate minerals. *Modern Geology*, 1, 283-300.
- Hunt G.R., Salisbury J.W. 1971. Visible and near-infrared spectra of minerals and rocks: II Carbonates. *Modern Geology*, 2, 23-30.
- Hunt G.R., Salisbury J.W., Lenhoff C.J. 1971a. Visible and near-infrared spectra of minerals and rocks: III Oxides and hydroxides. *Modern Geology*, 2, 195-205.
- Hunt G.R., Salisbury J.W., Lenhoff C.J. 1971b. Visible and near-infrared spectra of minerals and rocks: IV Sulphides and sulphates. *Modern Geology*, 3, 1-14.
- Hunt G.R., Ashley R.P. 1979. Spectra of altered rocks in the visible and near infrared. *Economic Geology*, 74, 1613–1629.
- Janikian L., Almeida R.P., Trindade R.F., Fragoso-Cesar A.R.S., D'Agrella-Filho M.S., Dantas E. L., Tohver E. 2008. The continental record of Ediacaran volcano-sedimentary successions in southern Brazil and their global implications. *Terra Nova*, 20, 259-266.
- Janikian L., Almeida R.P., Fragoso-Cesar A.R.S., Martins U.T.S., Dantas E.L., Tohver E., McCreath I., D'Agrella-Filho M.S. 2012. Ages (U-Pb SHRIMP and LA ICPMS) and stratigraphic evolution of the Neoproterozoic volcano-sedimentary successions from the extensional Camaquã Basin, Southern Brazil. *Gondwana Research* 21, 466–482.
- Kelley, K.D., Spry, P.C., McLemore, V.T., Fey, D.L., and Anderson, E.D., 2020, Alkaline-type epithermal gold deposit model: U.S. Geological Survey Scientific Investigations Report 2010–5070–R, 74 p., <https://doi.org/10.3133/sir20105070R>.
- Kokaly R.E., Clark R.N., Swayze G.A., Livo K.E., Hoefen T.M., Pearson N.C., Wise R.A., Benzel W.M., Lowers H.A., Driscoll R.L., Klein A.J. 2017. USGS Spectral Library Version 7: U.S. Geological Survey Data Series 1035, 61 p., <https://doi.org/10.3133/ds1035>.
- Laux J. H., Lindenmeyer Z. G.; Teixeira J.B.G., Neto, A.B. 2005 Ore genesis at the Camaquã copper mine, a Neoproterozoic sediment-hosted deposit in Southern Brazil. *Ore Geology Reviews*, 26, 71-89.
- Leinz V., Barbosa A.F., Teixeira E. 1941. Mapa Geológico Caçapava-Lavras. Secretaria da Agricultura, Indústria e Comércio-RS. Boletim 90, 39p
- Lima E.F., Nardi, L.V.S. 1998. The Lavras do Sul shoshonitic association: implications for the origin and evolution of Neoproterozoic shoshonitic magmatism in the southernmost Brazil. *Journal of South American Earth Sciences*, 11, 67-77.
- Lopes C.G., Pimentel M.M., Philipp R.P., Gruber L., Armstrong R., Junges, S. 2015. Provenance of the Passo Feio complex, Dom Feliciano belt: implications for the age of supracrustal rocks of the São Gabriel arc, southern Brazil. *Journal of South American Earth Sciences*, 58, 9–17.
- Marconato A. 2010. A influência da evolução de altos estruturais em sucessões aluviais: exemplos do Ediacarano e do Cambriano da Bacia Camaquã (RS). MSc Dissertation, Instituto de Geociências, Universidade de São Paulo, São Paulo. <https://www.teses.usp.br/teses/disponiveis/44/44141/tde-31052010-155303>.
- Martins G.S., Fragoso-Cesar A.R.S., Carvalho V.O. 2009. A Zona de Cisalhamento Cerro dos Andradas e sua Implicação Tectônica na Estratigrafia da Bacia do Camaquã (Ediacarano-Eocambriano do Rio Grande do Sul). In: *Simpósio Nacional de Estudos Tectônicos (SNET)*, 12, p. 79.
- Matté V., Sommer C.A., Lima E.F., Philipp R.P., Basei M.A.S. 2016. Post-collisional Ediacaran volcanism in oriental Ramada Plateau, southern Brazil. *Journal of South American Earth Sciences*, 71, 201-222.
- Matté V., Sommer C.A., Lima E.F. 2021. O vulcanismo ediacarano-cambriano da Bacia Camaquã. In: Jelinek A.R., Sommer C.A. (eds.) *Contribuições à geologia do Rio Grande do Sul e Santa Catarina. Publicação Especial do Núcleo RS/SC da Sociedade Brasileira de Geologia SBG*, Porto Alegre, p. 129-148. <https://doi.org/10.29327/537860>
- Melcher G., Mau H. 1960. Novas observações geológicas na região de Caçapava do Sul, Rio Grande do Sul. *Anais da Academia Brasileira de Ciências*, 32, 43-50.
- Mexias, A.S., Bongioiolo, E.M.; Gomes, M.E.B., Formoso, M.L.L., Frantz, J.C. 2007. Alterações hidrotermais e mineralizações nas rochas da associação plutono-vulcano-sedimentar da região de Lavras do Sul-RS. In: Ianuzzi R., Frantz J. C. (org.) *50 Anos de Geologia: Instituto de Geociências, contribuições*. Porto Alegre, Comunicação e Identidade, p. 143-159.



- Misi A., Kaufman A.J., Veizer J., Powis K., Azmy, K., Boggiani P.C., Gaucher C., Teixeira, J.B.G., Sanches A.L., Iyer S.S.S. 2007. Chemostratigraphic correlation of Neoproterozoic successions in South America. *Chemical Geology*, 237, 143-167.
- Nardi L.V.S., Bitencourt M.F. 1989. Geologia, petrologia e geoquímica do Complexo Granítico Caçapava do Sul, RS. *Revista Brasileira de Geociências*, 19, 153-269.
- Paim P.S.G., Chemale Jr. F., Lopes R.C. 2000. A Bacia do Camaquã. In: Holz M., De Ros L.F. (eds.) *Geologia do Rio Grande do Sul*. Porto Alegre, UFRGS/CIGO. p. 231- 274.
- Paim P.S.G., Chemale Jr. F., Wildner W. 2014. Estágios evolutivos da Bacia do Camaquã (RS). *Ciência & Natura*, 36, 183-193.
- Passos N., Gavronski E.F., Azevedo J.G. 1959. Relatório sobre prospecção das ocorrências de cobre de Cerro dos Andradas, Primavera e Santa Bárbara no Município de Caçapava do Sul, Rio Grande do Sul. Porto Alegre, DNPM, 43 p.
- Philipp R.P., Pimentel M.M., Basei M.A.S., Salvi M., Lena L.O.F., Vedana L.A., Gubert M.L., Lopes C.G., Laux J.H., Camozzato E. 2021. U-Pb detrital zircon dating applied to metavolcano-sedimentary complexes of the São Gabriel Terrane: new constraints on the evolution of the Dom Feliciano Belt. *Journal of South America Earth Sciences*, 110, 103409.
- Pontual S., Merry N.J., Gamson, P. 2008. *Spectral Interpretation Field Manual*. 3.ed. (GMEX Guides for Mineral Exploration, 1). Australia, Ausspec International, 189 p.
- Remus M.V.D., Hartmann L.A. 1997. Caracterização do minério do Depósito Santa Barbara-Rosso, Caçapava do Sul — RS. In: *Caracterização de Minérios e Rejeitos de Depósitos Minerais Brasileiros, Resumos Expandidos*, DNPM/DIREX, PADCT/GTM, Ministério das Minas e Energia, Brasília, Brasil. p. 91-98.
- Remus M.V.D., Hartmann L.A., McNaughton N.J., Groves D.I., Fletcher I.R. 2000a. The link between hydrothermal epigenetic copper mineralization and the Caçapava Granite of the Brasiliano Cycle in Southern Brazil. *Journal of South America Earth Sciences*, 13, 191-216.
- Remus M.V.D., Hartmann L.A., McNaughton N.J. Groves D.I., Reisch J.L. 2000b. Distal magmatic-hydrothermal origin for the Camaquã Cu (Au-Ag) and Santa Maria Pb, Zn (Cu-Ag) Deposits, Southern Brazil. *Gondwana Research*, 3, 155-174.
- Renac C., Mexias A.S., Gomes M.E.B., Ronchi L.H., Nardi L.V.S., Laux, J. H. 2014. Isotopic fluid changes in a Neoproterozoic porphyry-epithermal system: The Uruguay mine, southern Brazil. *Ore Geology Reviews*, 60, 146-160.
- Ribeiro M.J., Bocchi P.R., Figueiredo F.P.M. 1966. *Geologia da quadrícula de Caçapava do Sul, Rio Grande do Sul - Brasil*. Boletim DNPM, Rio de Janeiro, n. 127.
- Ribeiro M. J. 1978. Mapa previsional do cobre no Escudo Sul-Rio-Grandense: nota explicativa. (Boletim Geológico, n. 3, Seção Geologia Econômica, n. 1). Brasília, DNPM/DFPM, 104 p.
- Ribeiro M.J. 1991. Sulfetos em sedimentos detríticos cambrianos do Rio Grande do Sul, Brasil. PhD Thesis, Instituto de Geociências, Universidade Federal do Rio Grande do Sul, Porto Alegre, 416 p.
- Roache T.J., Walshe J.L., Huntington J.F., Quigley M.A., Yang K., Bil B.W., Blake K.L., Hyvärinen, T. 2011. Epidote-clinozoisite as a hyperspectral tool in exploration for Archean gold. *Australian Journal of Earth Sciences*, 58, 813-822.
- Robertson J., Johnson R. 1966. Copper deposits of Caçapava do Sul-Lavras do Sul Region. MMF-USGS - BR 8
- Sillitoe, R. H., Hedenquist, J. W., 2003. Linkages between volcanotectonic settings, ore-fluid compositions, and epithermal precious metal deposits. Book Chapter 16 in: Simmons S.F.; Ian Graham I. (Editors). *Volcanic, Geothermal, and Ore-Forming Fluids: Rulers and Witnesses of Processes within the Earth*. *Economic Geology*, Society of Economic Geologists, 10, 315-343.
- Simmons, S. F., White, N. C., & John, D. A., 2005. Geological characteristics of epithermal precious and base metal deposits. Book Chapter in: Hedenquist, J. W.; Thompson, J. F. H., Goldfarb, R.J. Richards, J. P. *One Hundredth Anniversary Volume. Economic Geology*, Society of Economic Geologists.
- Silva-Filho B.C., Matsdorf M., 1987. Análise estrutural dos metamorfitos da borda oeste do Granito Caçapava, Caçapava do Sul: implicações geológicas locais e regionais. In: *Simpósio Sul-Brasileiro de Geologia*, 3.
- Sommer C.A., Lima E.F., Nardi L.V.S., Liz J.D., Waichel B.L. 2006. The evolution of Neoproterozoic magmatism in southernmost Brazil: shoshonitic, high-K tholeiitic and silicasaturated, sodic alkaline volcanism in postcollisional basins. *Anais da Academia Brasileira de Ciências*, 78, 573-589.
- Souza, T. L 2020. *Genese dos serpentinitos e esteatitos do Complexo Passo Feio (RS, Brasil): evidências mineralógicas, geoquímicas e isotópicas*. Unpublished PhD Thesis, 204p. Programa de Pós-Graduação em Geociências, Universidade Federal do RS, Porto Alegre-RS.
- Teixeira G., Gonzales M.A. 1988. Minas do Camaquã, município de Caçapava do Sul, RS. In: Schobbenhaus C., C.E Silva C.E.C. (eds.) *Principais Depósitos Minerais do Brasil*, vol 3, DNPM/CVRD, Rio de Janeiro, 33-41 p.
- Toniolo J.A., Remus M.V.D., Reischl J.L. 2010. Depósito de cobre das Minas do Camaquã, Rio Grande Do Sul. In: Brito R.S.C., Silva M.G., Kuyumjian R.M. (org.). *Modelos de depósitos brasileiros de cobre do Brasil e sua resposta ao intemperismo*. Brasília, CPRM, 165-188 p.
- Toniolo J.A., Remus M.V.D. Macambira M.J.B., Moura C.A.V. 2004. Metalogênese do Depósito de Cobre Cerro dos Martins, RS: revisão e geoquímica isotópica de Sr, S, O e C. *Revista Pesquisas em Geociências*, 31, 41-67.
- Wang L., Qin K., Song G., Li G., 2019. A review of intermediate sulfidation epithermal deposits and subclassification, *Ore Geology Reviews*, 107, 434-456, <https://doi.org/10.1016/j.oregeorev.2019.02.023>.
- Wildner W., Lima E.F., Nardi L.V.S., Sommer C.A. 2002. Volcanic cycles and setting in the Neoproterozoic Ill to Ordovician Camaquã Basin succession in southern Brazil: characteristics of post-collisional magmatism. *Journal of Volcanology and Geothermal Research*, 118, 261-283.
- Wildner, W., Nardi, L.V.S., Lima, E.F. 1999. Postcollisional alkaline magmatism on the Taquarembó Plateau: a well preserved Neoproterozoic-Cambrian plutono-volcanic association in southern Brazil. *International Geology Review*, 41, 1082-1098.



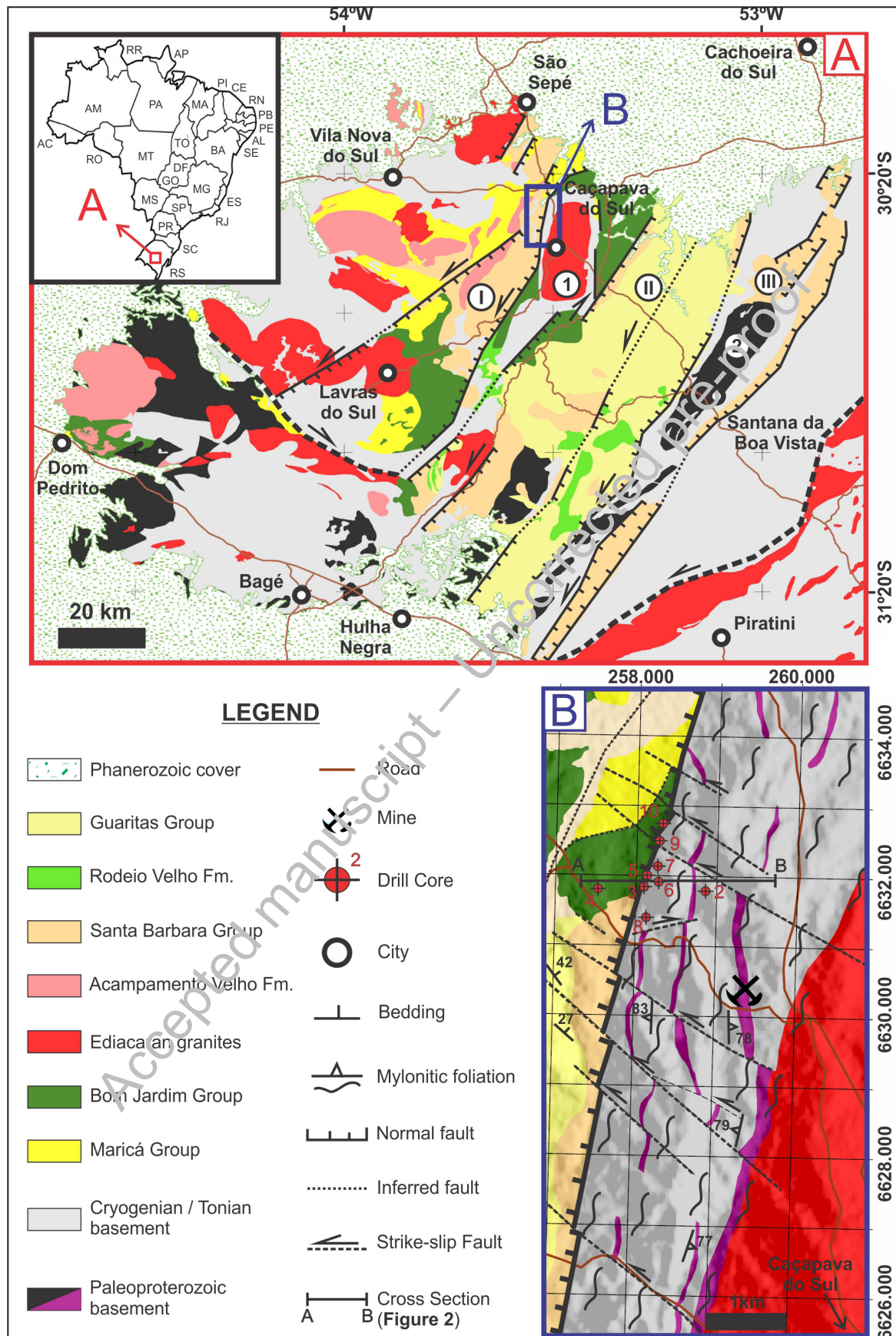


**FIGURE 1.** Location of the study area. (A) Regional tectonic location map (modified from Ribeiro, 1966, 1978; DNPM, 1989; Fragoço Cesar et al., 2000; CPRM, 2006; Almeida et al., 2012; Laux et al., 2021). (B) Local geological map (modified from Porcher et al, 1995).

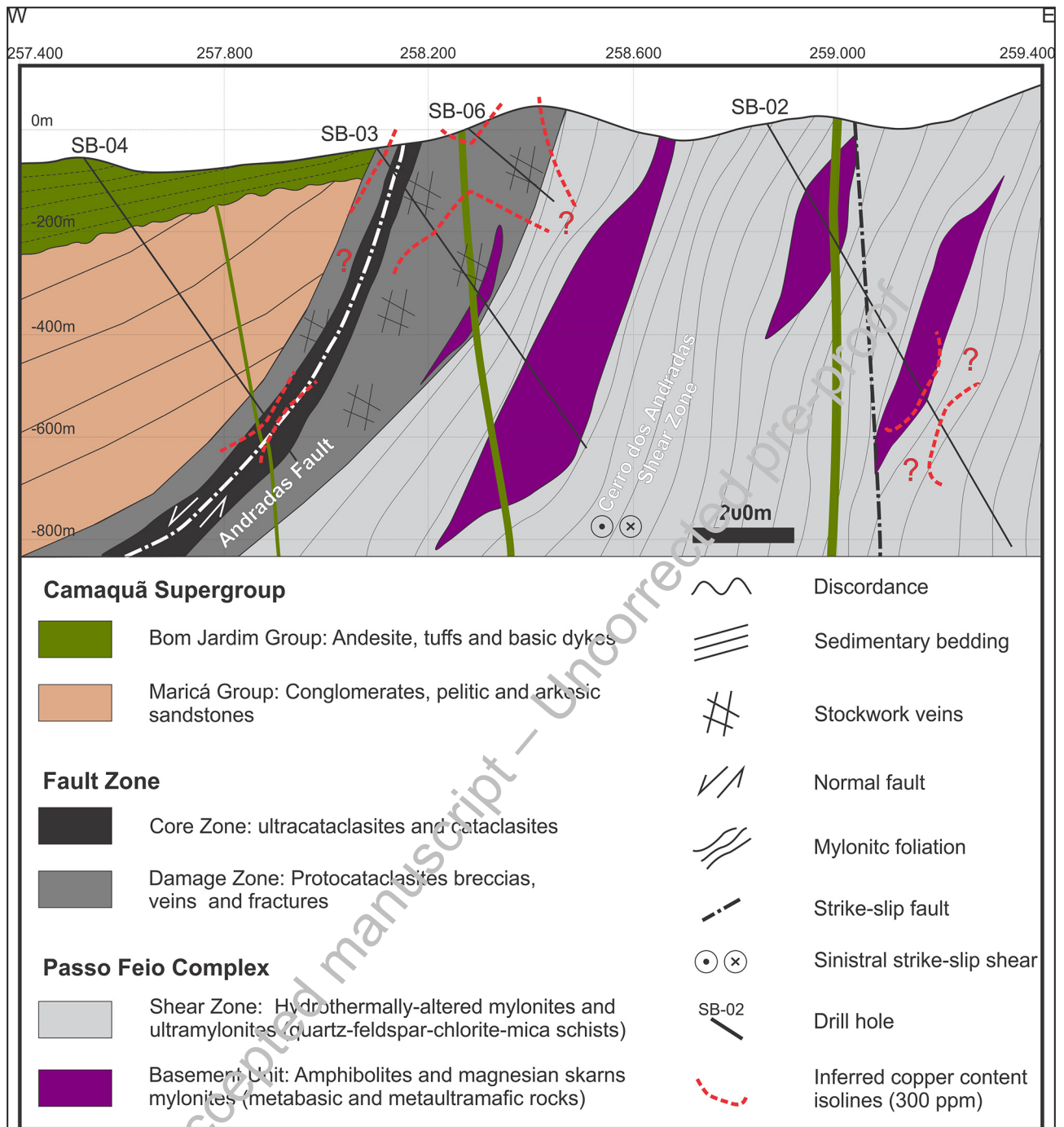


**FIGURE 2.** Simplified geological cross section A-B (see location in Figure 1), showing the main lithotypes found in the drill holes at the Santa Bárbara Deposit and the mineralization associated with the fault core and damage zones.



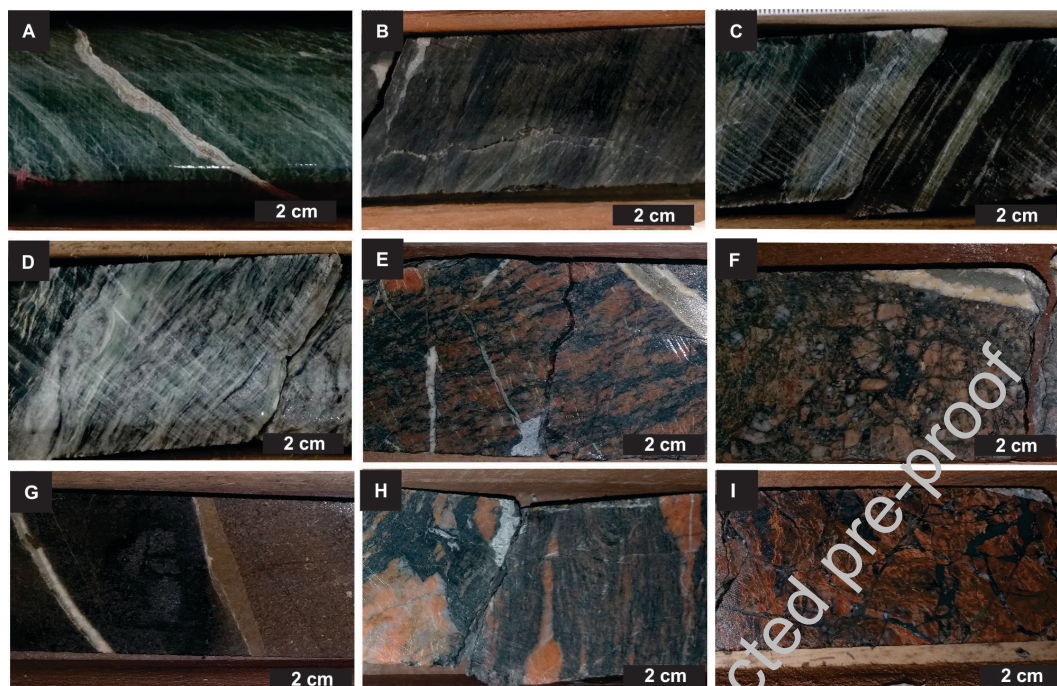


**FIGURE 3.** Main lithotypes found in drill holes at the Santa Bárbara Deposit. (A) Chlorite-quartz schist (SB-02-337m); (B) Muscovite-chlorite-quartz schist (SB-02-516m); (C) Interpolation of actinolite amphibolite (dark level) and talc-chlorite schist (light level) (SB-02-593m); (D) Talc-carbonate schist (SB-02-585m); (E) Chloritized quartz-feldspathic mylonite (SB-03-72m); (F) Chloritized quartz-feldspathic cataclasite (SB-09-31m). (G) Andesitic basalt with carbonate-alteration halo in core SB-08 (120m); (H) Chloritized quartz-feldspathic mylonite (SB-03-60m). (I) Chloritized quartz-feldspathic cataclasite (SB-09-69m).

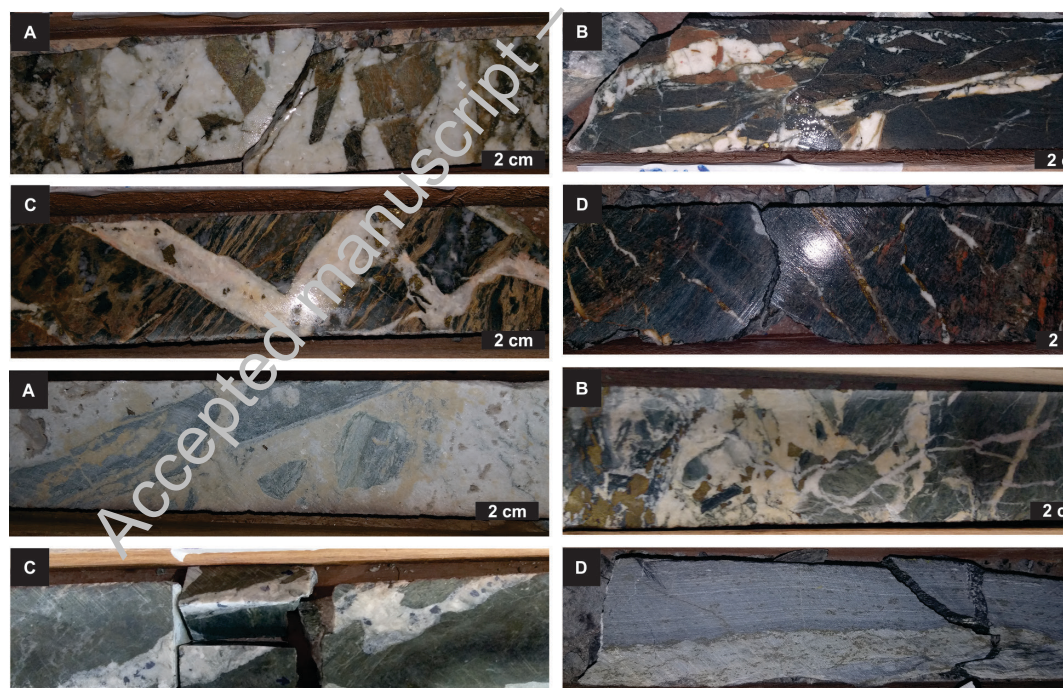


**FIGURE 4.** Detail of copper occurrences at the Santa Bárbara Deposit intercepted by drill holes. (A) Calcitic and Fe-dolomitic hydraulic breccia with fragments of argillized chlorite-quartz schist in core SB-09 (52m-); (B) Brecciated andesitic basalt with sulfide-bearing carbonate veins in core SB-08 (121m); (C) Sulfide-bearing calcitic and Fe-dolomitic with chalcopyrite vein cutting argillized chlorite-quartz schist in core SB-06 (161m); (D) Stockwork-style vein of sulfide-bearing carbonate composition with chalcopyrite cutting cataclastic and mylonitic chlorite schist quartz-feldspathic in core SB-03 (65m); (E) Fe-dolomitic and calcitic hydraulic breccia with fragments of chlorite-quartz schist (640m); (F) Sulfide-bearing Fe-dolomitic and calcitic hydraulic breccia with chalcopyrite within fragments of amphibolite (655m); (G) Sulfide-bearing carbonate vein with sphalerite and galena (644m); (H) Sericite-chlorite schist with concordant sphalerite and galena mineralization along mylonitic foliation (711m).



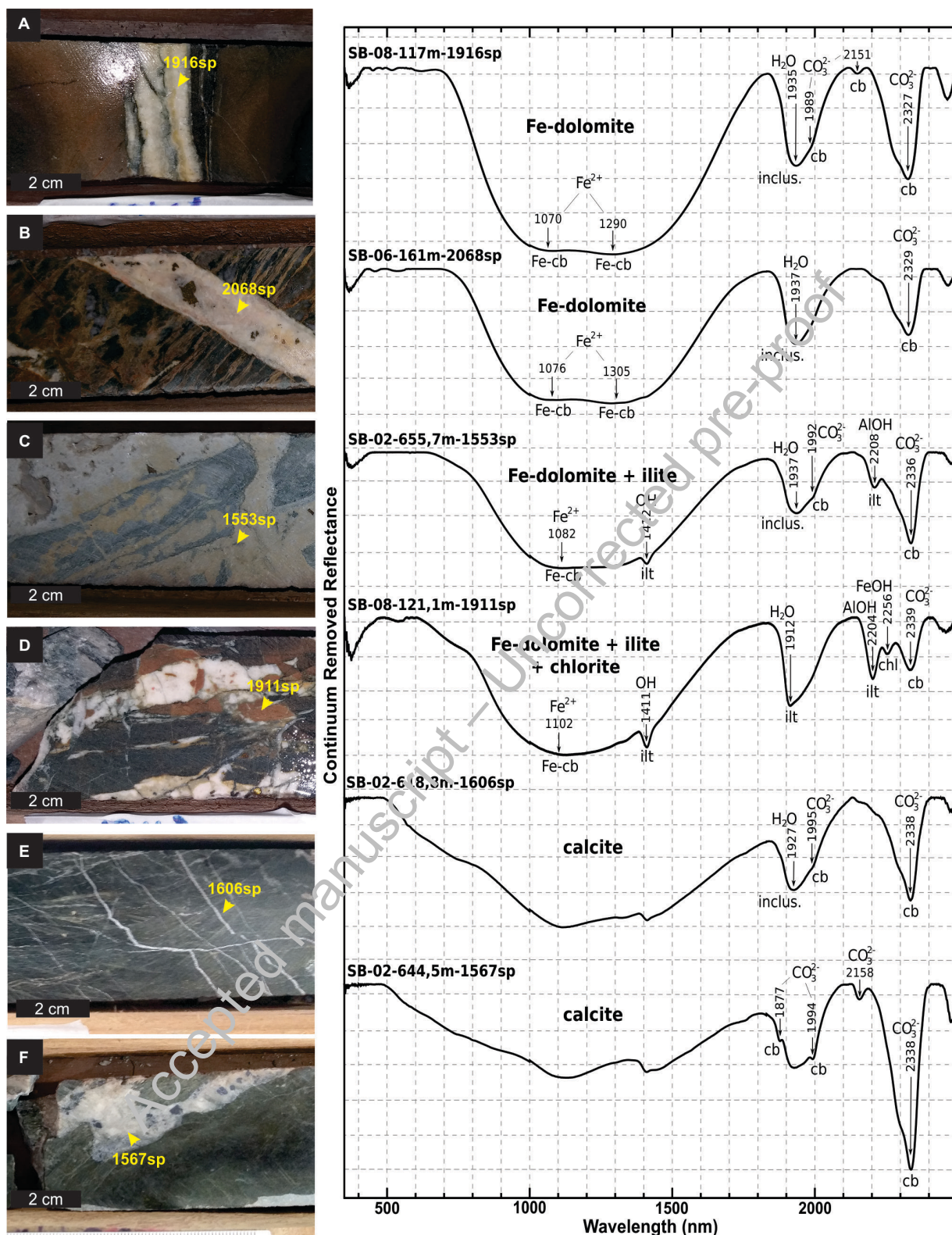


**FIGURE 5.** Carbonatization affecting the lithotypes at the Santa Bárbara Deposit and spectra of the lithological features. Arrows highlight the main absorption features, indicating the wavelength position, associated molecules/ions, and mineral interpretations. (A) Fe-carbonate vein with disseminated copper sulfides, colloform texture, and argillization halo, hosted in andesite (SB-08-117m-1916sp); (B) Sulfide-bearing calcitic and Fe-dolomitic with chalcopyrite vein cutting argillized chlorite-quartz schist in core SB-06 (161m-2068sp); (C) Sulfide-bearing Fe-dolomitic and calcitic hydraulic breccia with chalcopyrite within fragments of amphibolite (655m-1573sp); (D) Brecciated andesitic basalt with sulfide-bearing carbonate veins in core SB-08 (121m-1911sp); (E) Stockwork-style carbonate veining hosted in amphibolite (SB-02-619m-1606sp) within a lithochemical anomaly (Cu: 500ppm); (F) Sulfide-bearing carbonate vein with sphalerite and galena (644m-1567sp). Abbreviations: cb: carbonate; chl: chlorite; Fe-cb: Fe-carbonate; il: illite; inclus.: water-bearing fluid inclusion; sp = spectral analysis number.



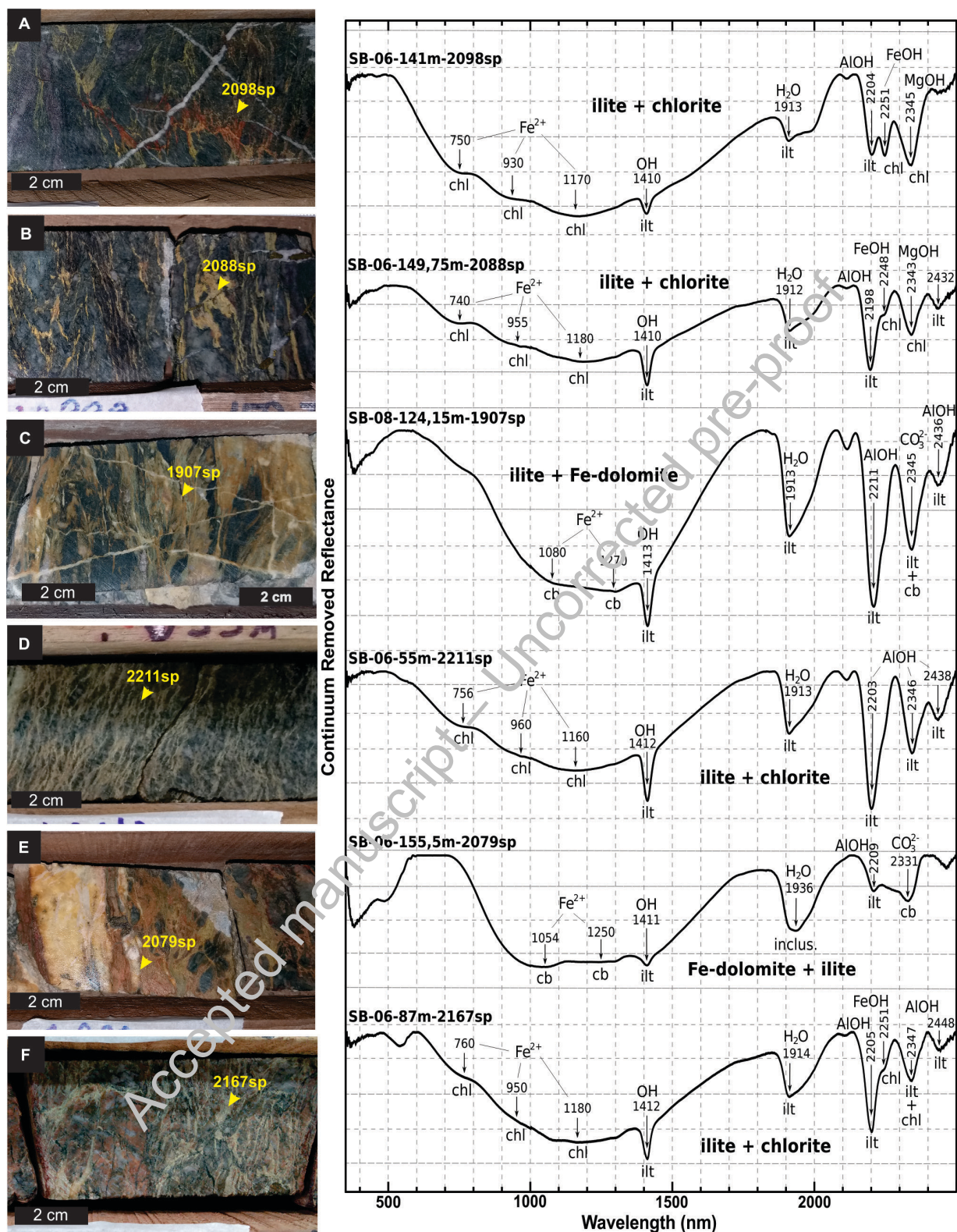


**FIGURE 6.** Argillization affecting the lithotypes at the Santa Bárbara Deposit and spectra of the lithological features. Arrows highlight the main absorption features, indicating the wavelength position, associated molecules/ions, and mineral interpretations. (A) Reddish fissural argillization cut by carbonate veining (SB-06-141m-2098sp); (B) Beige fissural argillization cut by chalcopyrite veins (SB-06-150m-2088sp); (C) Pervasive argillization with associated sericite, intersected by carbonate veining (SB-08-124m-1907sp); (D) Pervasive argillization parallel to mylonitic foliation (SB-06-55m-2211sp); (E) Carbonate vein with a illite-sericite alteration halo (SB-06-155m-2079sp); (F) Fissural argillization affecting both chloritized (green) and albitized (pink) portions (SB-06-87m-2167sp); Abbreviations: cb: carbonate; chl: chlorite; il: illite; inclus.: water-bearing fluid inclusion; sp: spectral analysis number.



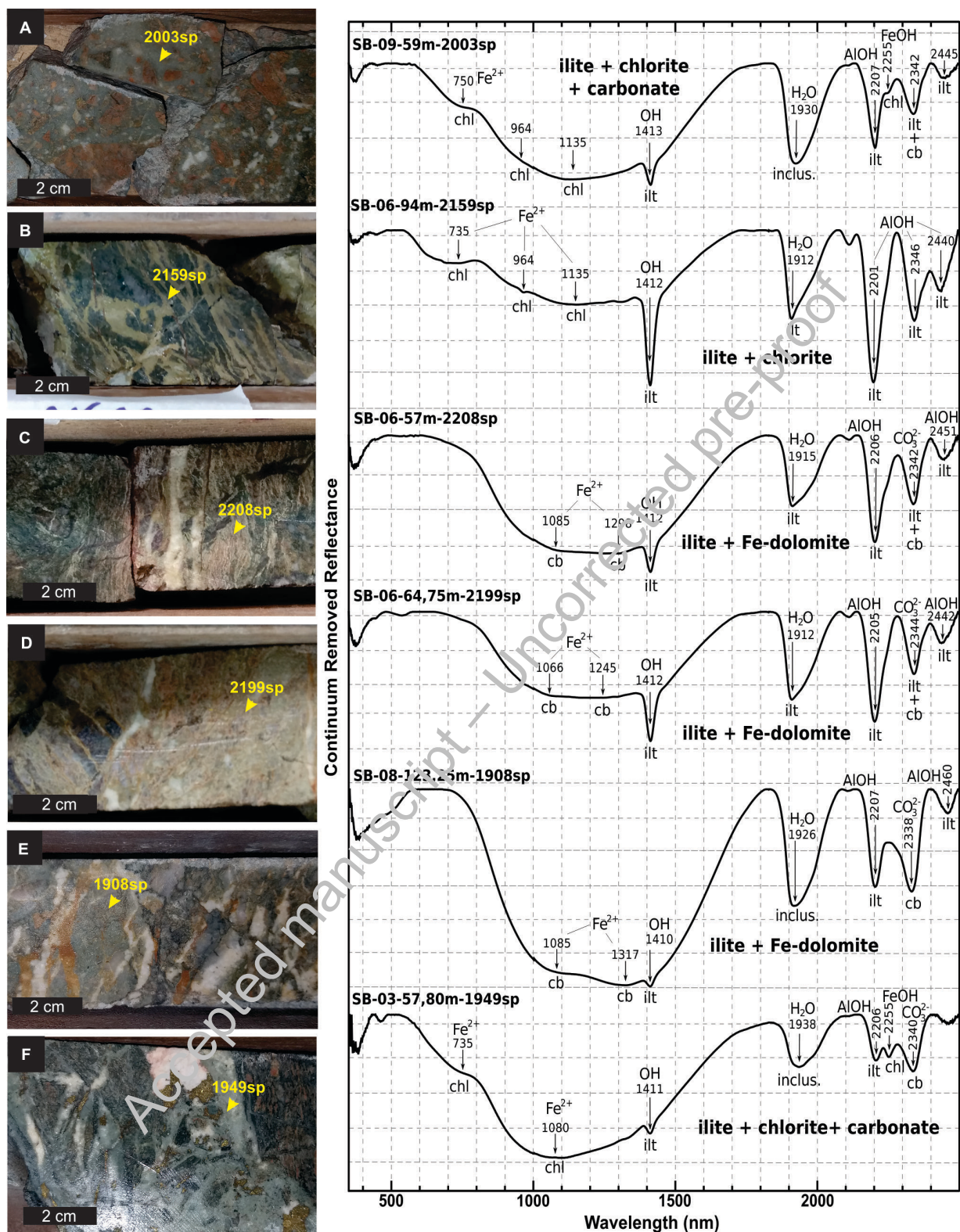


**FIGURE 7.** Argillization affecting the lithotypes at the Santa Bárbara Deposit and spectra of the lithological features. Arrows highlight the main absorption features, indicating the wavelength position, associated molecules/ions, and mineral interpretations. (A) Hydrothermal breccia with clay matrix and fragments of albitized and potassic rock (SB-09-53m-2003sp); (B) Fissural-pervasive argillization associated with a sulfide zone (SB-06-94m-2159sp); (C) Carbonate vein with a argillization halo (SB-06-57m-2208sp); (D) Generalized pervasive argillization associated with a carbonate vein (SB-06-65m-2199sp); (E) Fissural argillization in a silicified zone (SB-08-124m-1908sp); (F) Sulfide vein with associated silicification and gray argillization (SB-09-58m-1949sp). Abbreviations: cb: carbonate; chl: chlorite; ilt: illite; inclus.: water-bearing fluid inclusion; sp: spectral analysis number.



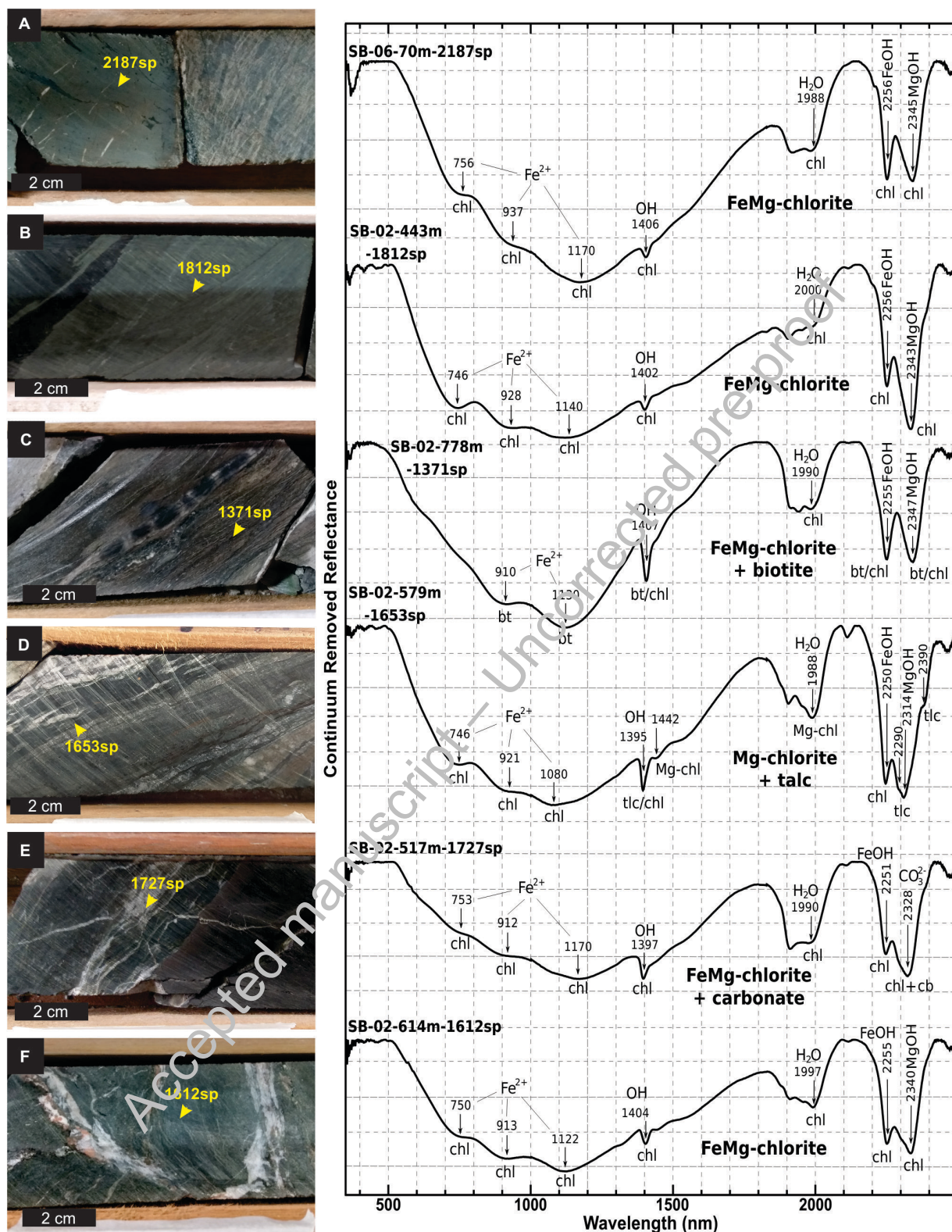
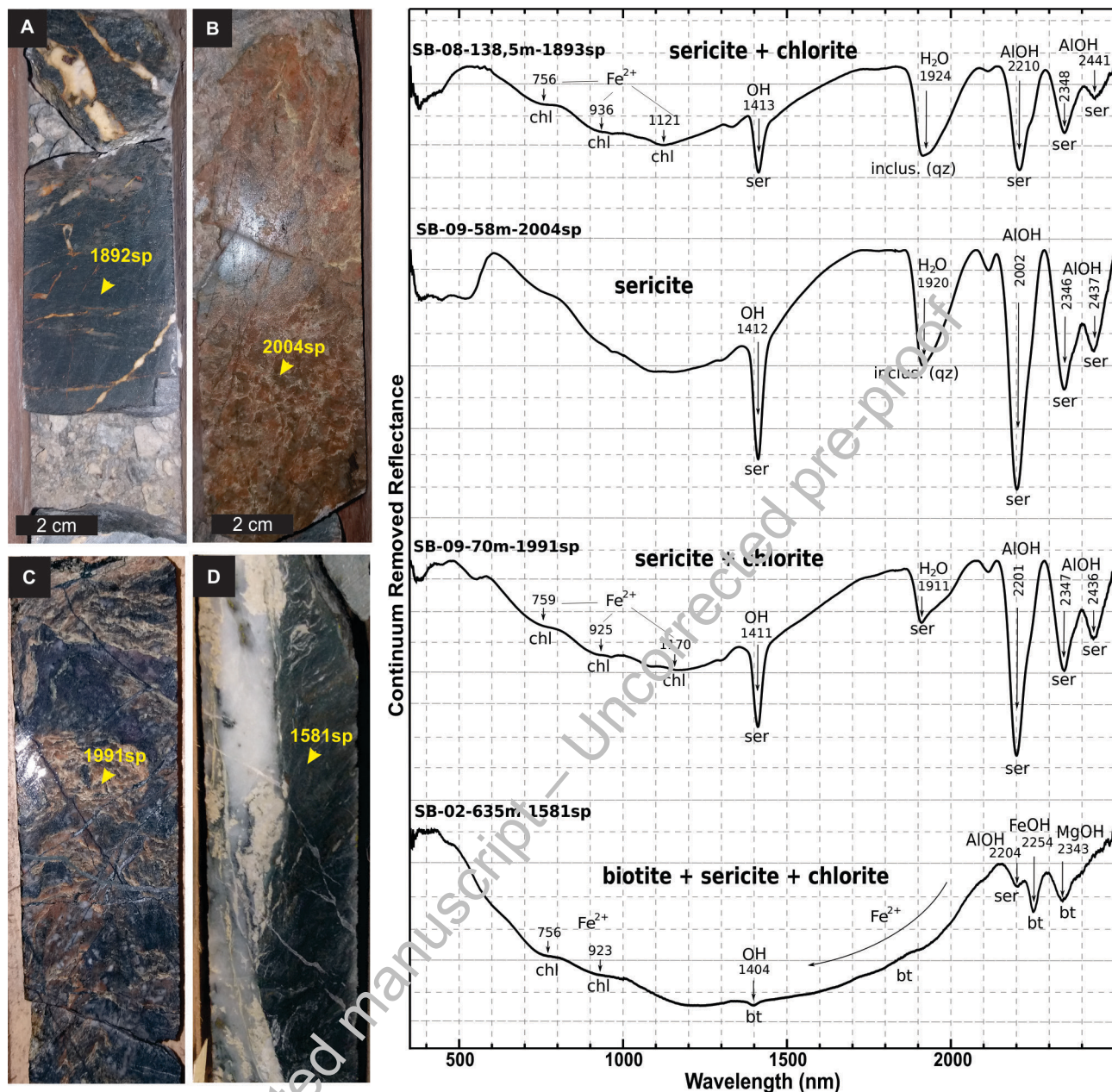


FIGURE 8. (A) Graph showing the variation in crystallinity of the sericite-illite-smectite series based on the ratio between the depths of absorption features related to AlOH and H<sub>2</sub>O, about the Cu concentrations (ppm) in the drill cores of the Santa Bárbara Deposit; (B) Graph showing the compositional variation of illite-sericite based on the wavelength position of AlOH absorption, about the Cu concentrations (ppm) in the drill cores of the Santa Bárbara Deposit; (C) Graph showing the compositional variation of chlorites based on the wavelength position of FeOH absorption, about the Cu concentrations (ppm) in the drill cores of the Santa Bárbara Deposit.





**FIGURE 9.** Chloritization affecting the lithotypes at the Santa Bárbara Deposit and spectra of the lithological features. Arrows highlight the main absorption features, indicating the wavelength position, associated molecules/ions, and mineral interpretations. (A) Pervasive alteration in mylonitic quartz-chlorite schist (SB-06-70m-21871sp); (B) Pervasive alteration in mylonitic quartz-chlorite schist (SB-02-443m-1812sp); (C) Selective pervasive alteration in mylonitic muscovite-biotite quartz-feldspathic schist (SB-02-778m-1371sp); (D) Selective pervasive alteration in talc schist and banded mylonitic amphibolite (SB-02-579m-1653sp); (E) Fissural alteration associated with carbonate veins, cutting through mylonitic quartz-chlorite schist and amphibolite (SB-02-517m-1727sp); (F) Fissural alteration associated with carbonate veins cutting through amphibolite (SB-02-614m-1612sp). Abbreviations: bt: biotite; cb: carbonate; chl: chlorite; Mg-chl: Mg-chlorite; tlc: talc; sp: spectral analysis number.



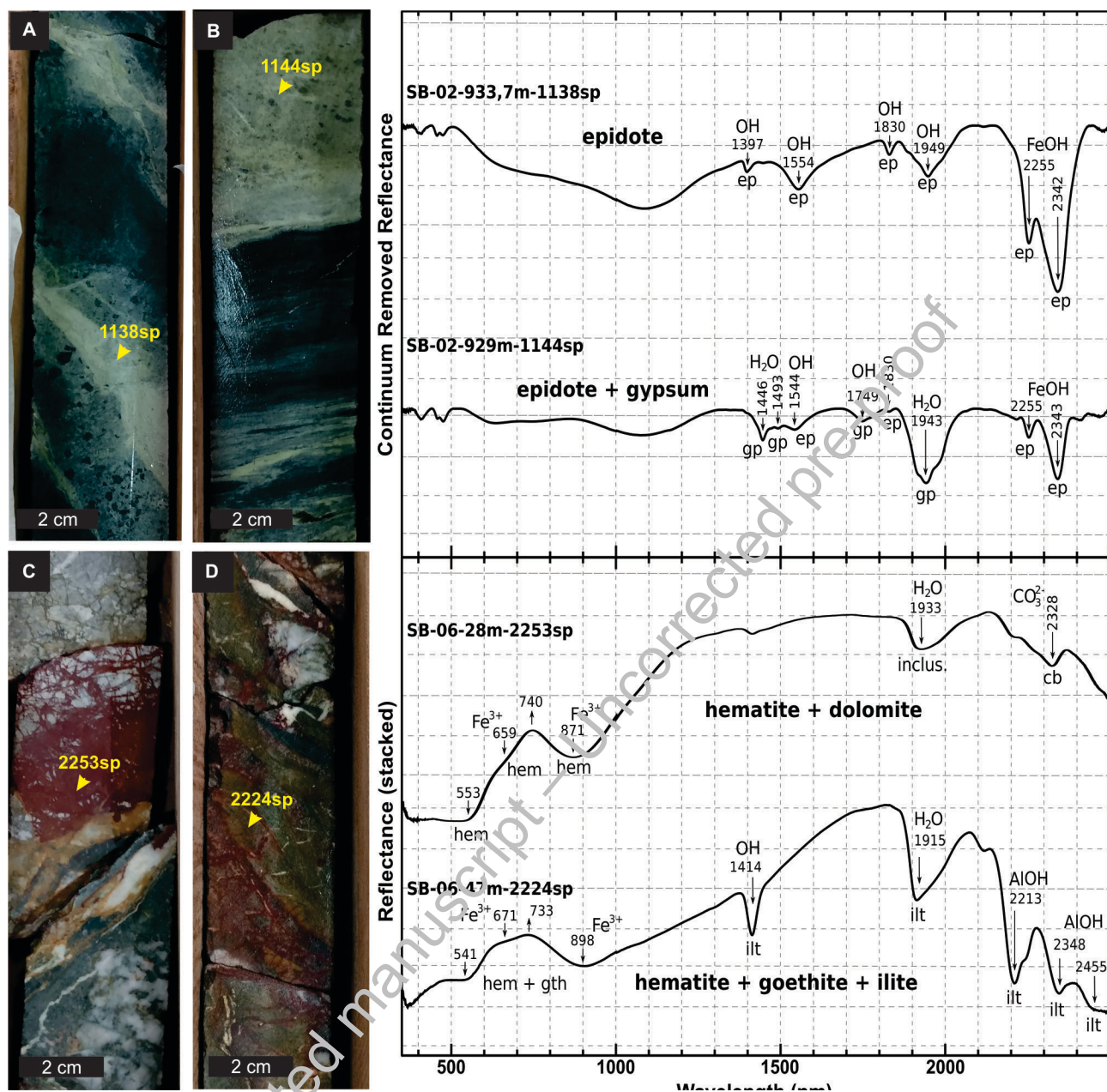


**FIGURE 10.** Sericitization affecting the lithotypes at the Santa Bárbara Deposit and spectra of lithological features. Arrows highlight the main absorption features, indicating the wavelength position, associated molecules/ions, and mineral interpretations. (A) Chloritized and sericitized quartz-feldspathic mylonite (SB-08-138m-1893sp); (B) albitized and sericitized chlorite quartz-feldspar schist, (SB-09-58m-2004sp); (D) Selective pervasive alteration in mylonitic quartz-chlorite schist (SB-02-631m-1581sp); (C) Pervasive alteration in chlorite quartz-feldspathic schist, albitized and sericitized, intersected by carbonate veinlets (SB-09-70m-1991sp). Abbreviations: bt: biotite; chl: chlorite; inclus.: water-bearing fluid inclusion; ser: sericite; sp: spectral analysis number.

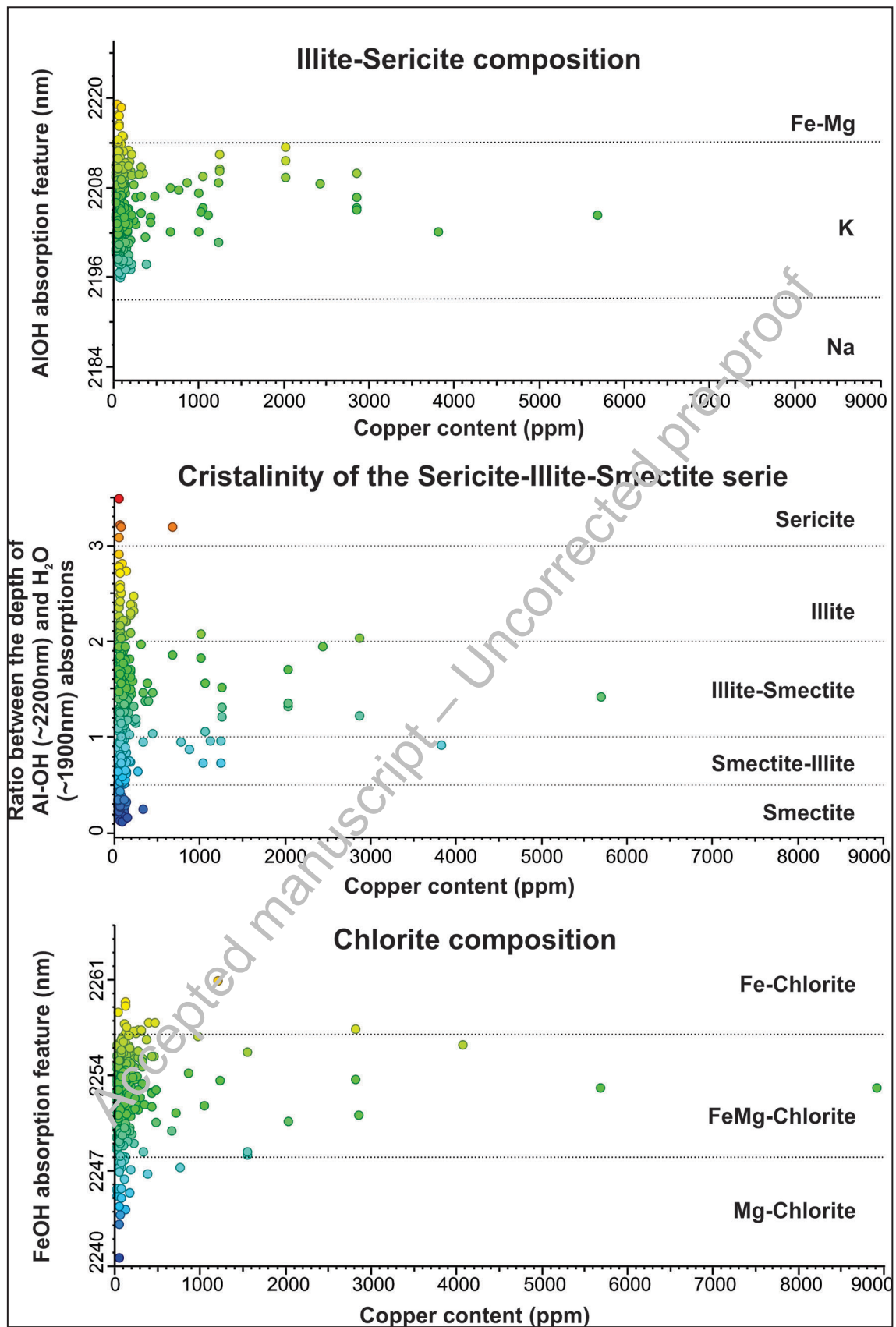


**FIGURE 11.** Core section from drill-hole SB-09 at the Santa Bárbara Deposit, Between Depths of 45m and 65m (Left to Right). This section shows pervasive potassic and albitic alteration (red and pink colors), overlaid by carbonate fissure zones (white) and illite-rich areas (beige), along with pervasive chloritization (dark gray). Abbreviations: fk+ab: feldspar and albite alteration; ill+cb: illite and carbonate alteration; cb+sulf: sulfide-bearing carbonate alteration





**FIGURE 12.** Minor alteration types affecting the host rocks of the Santa Bárbara deposit and spectra of lithological features. Arrows highlight the main absorption features, indicating the wavelength position, associated molecules/ions, and mineral interpretations. (A) hornfels with hornblende porphyroblasts and greenish epidote alteration halo (SB-02-872m-1227sp); (B) epidote-rich veins with gypsum and zeolite hosted in amphibolites (SB-02-933m-1138sp); (D) reddish hematite-goethite alteration veins associated with the green clay zone (SB-06-47m-2224sp); (C) reddish hematite-goethite-rich vein with brecciated and stockwork textures (SB-06-28m-2253sp). Abbreviations: cb: carbonate; chl: chlorite; dol: dolomite; ep: epidote; gp: gypsum; hbl: hornblende; hem: hematite; inclus.: water-bearing fluid inclusion; ser: sericite; tlc: talc; zeo: zeolite; sp: spectral analysis number.



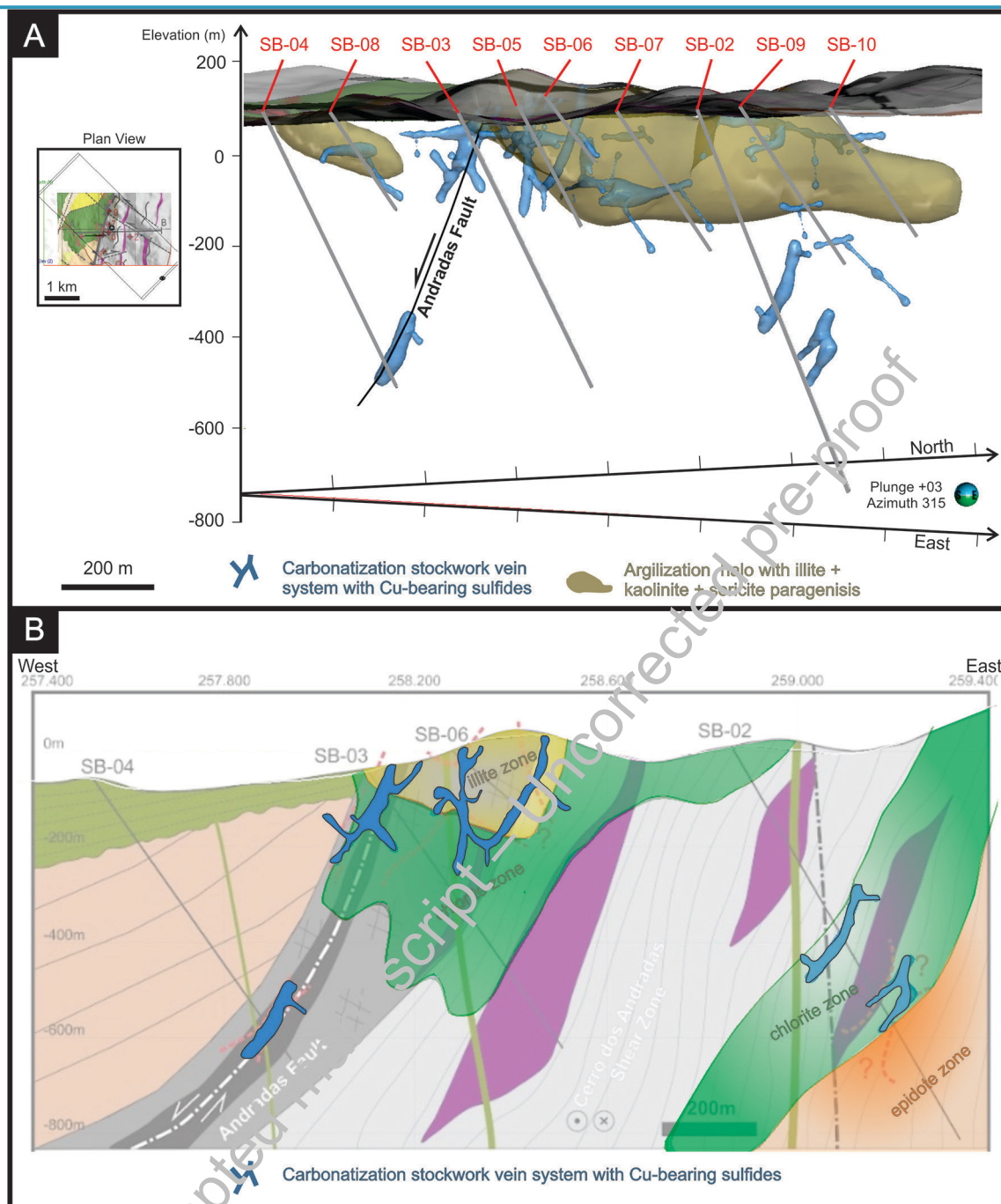


**FIGURE 13.** Model of alteration zones of the Santa Bárbara deposit. (A) 3D hydrothermal model showing epithermal carbonation stockwork vein system and argillization halo; (B) 2D hydrothermal model superposed on geological profile showed in Figure 2.

**TABLE 1.** Location and drilling information for the drill cores used to describe the Santa Bárbara deposit

Drill Hole	UTM East	UTM North	Zone	Azimuth	Dip	Depth (m)
SB-02	258862,81	6631793,33	22J	90	-60	953,70
SB-03	258102,14	6631833,11	22J	90	-55	708,18
SB-04	257530,61	6631800,62	22J	90	-55	714,34
SB-05	258133,05	6632001,34	22J	90	-55	297,25
SB-06	258281,66	6631912,79	22J	90	-40	212,80
SB-07	258264,37	6632137,78	22J	80	-50	407,35
SB-08	258136,42	6631399,96	22J	90	-45	290,85
SB-09	258286,31	6632495,09	22J	80	-50	449,55
SB-10	258320,59	6632743,81	22J	80	-50	362,50

**TABLE 2:** Geochemical results for nine anomalous metals at the Santa Bárbara deposit. The sections were sampled by the mineral prospecting company and analyzed by the Intertek laboratory. Source: Mining Ventures and Intertek reports. Abbreviations: NA: not analyzed; LD: Detection limit.

Drill Hole	Interval section (m)	Cu	Zn	Pb	As	Au*	Ag	Sn	Mo	W
SB-02	468 a 469,5	86	311	19	<LD	<LD	<LD	281	<LD	<LD
	490 a 491,5	52	1758	438	<LD	<LD	<LD	4	<LD	<LD
	640,64 a 641,33	6662	51	<LD	16	<LD	<LD	<LD	<LD	<LD
	647 a 648	98	1031	117	299	<LD	<LD	<LD	<LD	<LD
	650 a 651	48	1120	136	<LD	<LD	<LD	5	<LD	<LD
	655,22 a 656,44	1181	17	<LD	<LD	6	<LD	<LD	<LD	<LD
	656,44 a 657	1163	67	<LD	<LD	6	<LD	<LD	<LD	<LD
	657 a 658	2792	54	<LD	<LD	8	<LD	<LD	<LD	<LD
	707 a 708	264	6544	3186	124	<LD	<LD	<LD	18	116
	708 a 709	236	2451	1184	2134	14	<LD	<LD	15	21
	713 a 714	115	2117	860	41	<LD	<LD	<LD	<LD	18
	771 a 772	65	113	<LD	<LD	1842	<LD	<LD	<LD	<LD
	774 a 775	31	127	80	39	<LD	<LD	<LD	151	<LD
	775 a 776	65	3618	747	482	<LD	<LD	<LD	67	<LD
	827,14 a 828	55	69	<LD	<LD	10	748	3	<LD	<LD
SB-03	57 a 58	5650	50	<LD	<LD	10	<LD	NA	<LD	<LD
	59 a 60	2400	40	<LD	<LD	10	<LD	NA	<LD	<LD
	64 a 65	2830	40	<LD	<LD	30	<LD	NA	<LD	<LD
SB-05	74 a 75,5	1000	70	<LD	<LD	<LD	<LD	NA	<LD	<LD
SB-06	29 a 30,5	1710	40	<LD	<LD	10	<LD	NA	<LD	<LD
	51 a 52,1	1270	10	<LD	<LD	30	<LD	NA	<LD	<LD
	109 a 110,5	2130	50	<LD	<LD	10	<LD	NA	<LD	<LD
	138,5 a 140	1330	60	<LD	<LD	<LD	<LD	NA	<LD	<LD
	155,41 a 156,5	1160	20	<LD	<LD	<LD	<LD	NA	<LD	<LD
	158 a 159,5	2280	40	<LD	<LD	<LD	<LD	NA	<LD	<LD
	160,5 a 161,64	5220	30	<LD	<LD	30	<LD	NA	<LD	<LD
	206 a 207,5	1000	60	<LD	<LD	<LD	<LD	NA	<LD	<LD
SB-07	103,5 a 105	1990	20	<LD	<LD	<LD	<LD	NA	<LD	<LD
	105 a 106,5	1220	20	<LD	<LD	<LD	<LD	NA	<LD	<LD
	261,4 a 262,5	2700	30	<LD	<LD	<LD	<LD	NA	<LD	<LD
	262,5 a 263,5	1340	30	<LD	<LD	20	<LD	NA	<LD	<LD
	263,5 a 264,4	3070	30	<LD	<LD	60	<LD	NA	<LD	<LD
	363,5 a 365	2840	60	<LD	<LD	120	<LD	NA	10	<LD
SB-08	112 a 113,5	1080	60	<LD	<LD	<LD	<LD	NA	<LD	<LD
	118 a 119,5	1380	60	<LD	<LD	<LD	<LD	NA	<LD	<LD
	119,5 a 121	1210	60	<LD	<LD	<LD	<LD	NA	<LD	<LD
	122 a 123,15	4040	40	<LD	<LD	10	<LD	NA	<LD	<LD
	123,15 a 124,5	1020	40	<LD	<LD	30	<LD	NA	<LD	<LD
	138,66 a 139,92	8890	60	<LD	<LD	<LD	<LD	NA	<LD	<LD
SB-09	39 a 40,5	3790	10	<LD	<LD	<LD	<LD	NA	<LD	<LD
	40,5 a 41,5	2000	60	<LD	<LD	10	<LD	NA	10	<LD
	41,5 a 42,81	1520	10	<LD	<LD	<LD	<LD	NA	<LD	<LD
	52 a 53,5	1500	10	<LD	<LD	10	<LD	NA	<LD	<LD
	53,5 a 55	1000	10	<LD	<LD	<LD	2	NA	<LD	<LD
	125,55 a 126,5	1410	40	<LD	<LD	20	<LD	NA	<LD	<LD






**TABLE 3:** Hydrothermal zoning and the respective minerals identified by petrography and spectroscopy in the Santa Bárbara Target drill cores.

Hydrothermal zoning	Lithologies / Alteration Styles	Minerals identified by spectroscopy/petrography
Distal	pervasive alteration (chloritic)	chlorite, epidote, actinolite, (-) zeolite, (-) calcite
Proximal	fissural alteration with quartz-carbonate veins (sericitic and argillic)	muscovite, illite, montmorillonite, (-) chlorite, (-) calcite, (-) gypsum, (-) saponite
Mineralized	Cu and Fe sulphides-bearing quartz-carbonate breccias, veins and venules in stockwork zones (carbonate alteration)	ankerite, (-) gypsum, (-) chlorite, (-) calcite, (-) illite, (-) muscovite



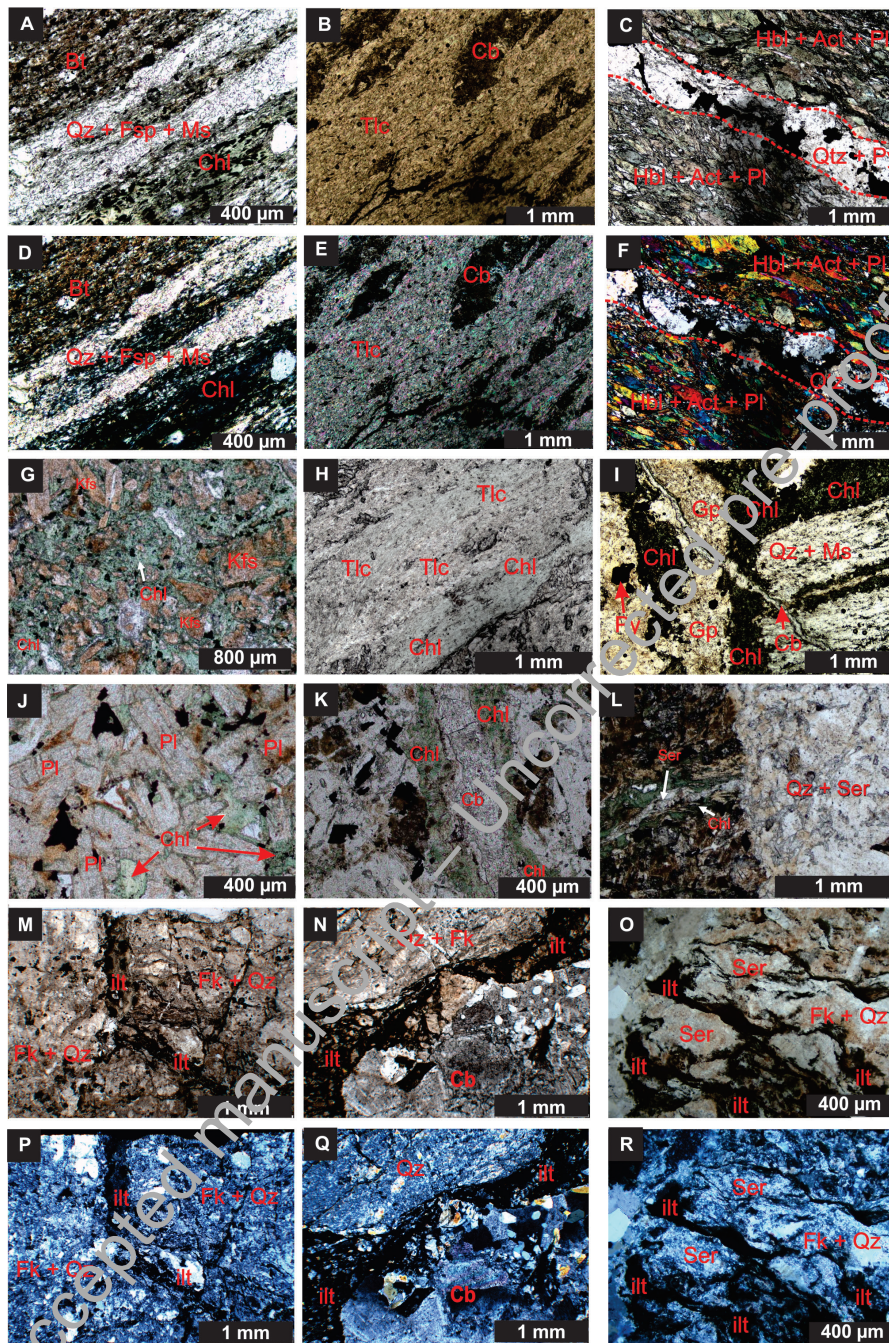
## Geology and hydrothermal alteration of the Santa Bárbara polymetallic deposit (Cu, Zn, Pb, Ag, Au): Insights into Ediacaran-Cambrian rift system evolution, Camaquã Basin, southern Brazil

Felipe Brito Mapa<sup>1,2,\*</sup> , Bruno Boito Turra<sup>1</sup> , João Luis Carneiro Naletto<sup>1</sup> , Rafael Gollanda Lazaro<sup>1</sup>,  
Guilherme Iolino Troncon Guerra<sup>1</sup> 

## APPENDIX

Accepted manuscript – Uncorrected pre-proof

## Appendix 1



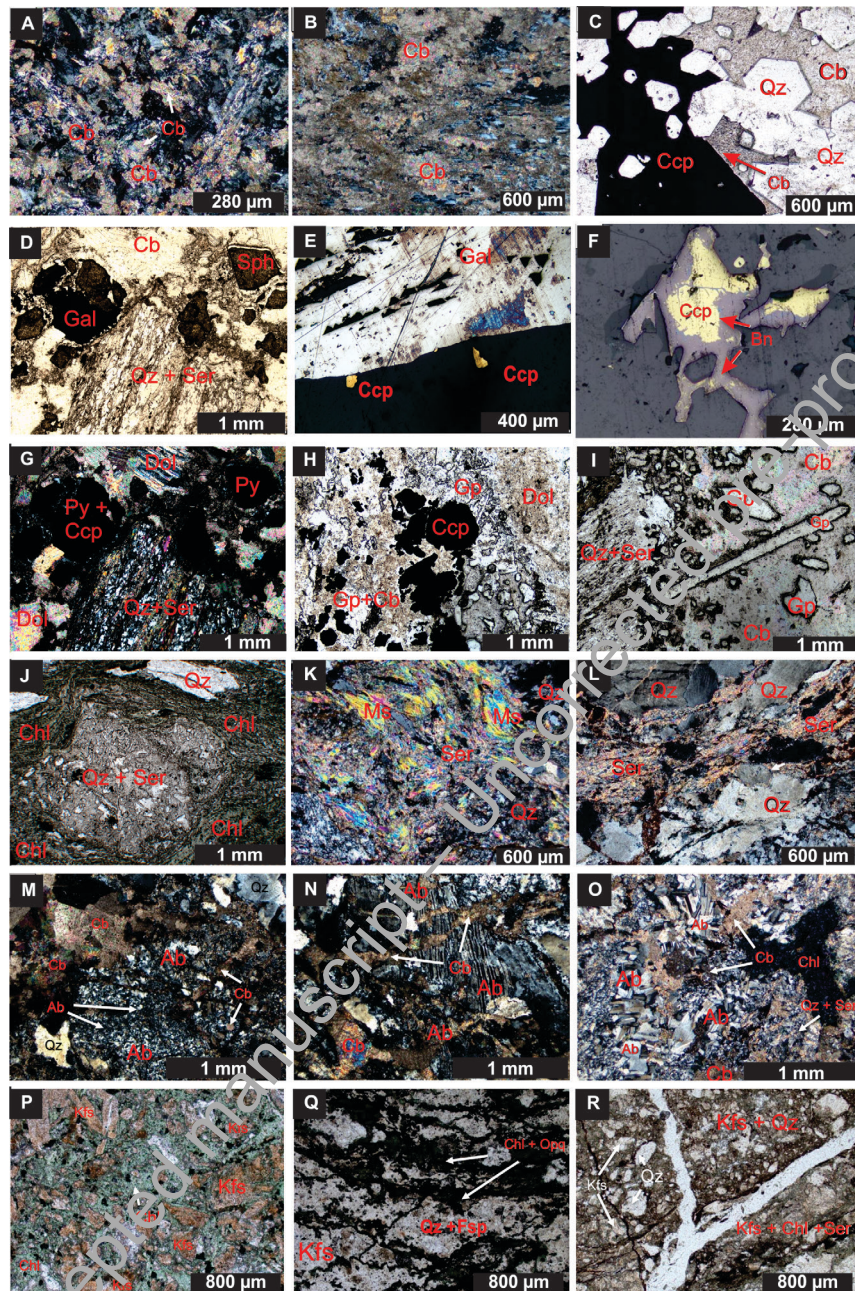
Photomicrographs of main lithotypes found in drill hole SB-02, and argillization and chloritization at the Santa Bárbara Deposit.

- (A) mylonitic muscovite-biotite-chlorite schist quartz-feldspathic (580m, LTP);  
 (B) mylonitic talc-carbonate schist (502m, LTP);  
 (C) mylonitic actinolite amphibolite (689m, LTP);  
 (D) Photomicrograph of (A) in LTC;  
 (E) Photomicrograph of (B) in LTC;  
 (F) Photomicrograph of (C) in LTC;  
 (G) Hydrothermal breccia (cataclasite) with pervasive chloritization (SB-08-119m-LTP); (H) Talc-chlorite schist (SB-02-219m-LTP);  
 (I) Fissural hydrothermal chlorite associated with a vein of sulfate, carbonate, and sulfide (SB-02-779m-LTP);  
 (J) Andesitic basalt with saussuritized plagioclase and interstitial hydrothermal chlorite (SB-08-119m-LTP);  
 (K) Fissural hydrothermal chlorite associated with a carbonate vein (SB-08-120m-LTP);  
 (L) Fissural hydrothermal chlorite associated with quartz and sericite veinlets (SB-08-122m-LTP).  
 (M) Hydrothermal breccia with fragments of potassic quartz-feldspathic rock and argillization fissure zones (SB-09-56m, LTP);  
 (N) Detail of a carbonate vein wall with ultracataclasite and clay matrix (SB-09-60m, LTP);  
 (O) Sericitized proto-cataclastic quartz-feldspathic breccia with argillization fissure zones (SB-09-56m, LTP);  
 (P) Image of (M) in LTC;  
 (Q) Image of (N) in LTC;  
 (R) Image of (O) in LTC.

Abbreviations: Ill: Illite; Ser: Sericite; Cb: Carbonates; Qtz: Quartz; Fk: Potassic Feldspar; LTP: Transmitted light, parallel polarizers; LTC: Transmitted light, crossed polarizers; LRP: Reflected light, parallel polarizers.



## Appendix 2



Photomicrographs of carbonatization associated with sulfation, sericitization and sodium and potassic alteration at the Santa Bárbara Deposit.

- (A) Pervasive carbonatization in andesite with igneous phaneritic texture and preserved plagioclase pseudomorphs (SB-08-116m, LTC);  
 (B) Intense pervasive carbonatization near a sulfide-bearing carbonate vein, featuring anhedral calcite aggregates (SB-08-116m, LTC);  
 (C) Sulfide-bearing carbonate vein with euhedral quartz and chalcopyrite crystals (SB-08-122m, LTC);  
 (D) Sulfide-bearing carbonate vein with euhedral sphalerite and galena crystals (SB-02-502m, LTC);  
 (E) Detail of (D), showing galena crystal with small chalcopyrite crystals on the edge (SB-02-502m, LRP);  
 (F) Chalcopyrite replacing edges and fractures with bornite (SB-08-119m, LRP);  
 (G) Sulfide-bearing carbonate vein with poikiloblastic crystals of pyrite and zinc sulfide (SB-02-779m, LTC);  
 (H) Detail of a zinc-mineralized vein with banding of sulfides, sulfates, and Fe-carbonates (SB-02-779m, LTP);  
 (I) Detail of gypsum crystals at the edge of a zinc-mineralized vein (SB-02-779m, LTP);  
 (J) mylonitic Quartz-chlorite schist with a porphyroclast of sericitized quartz-feldspathic breccia (SB-02-651m, LTP);  
 (K) Sericitized hydrothermal breccia with muscovite porphyroclast (SB-08-138m, LTC);  
 (L) Silicified and sericitized tectonic breccia (SB-08-122m, LTC);  
 (M) Tectonic breccia with albitized fragments and small anhedral albite crystals, overlaid by pervasive carbonatization (SB-09-56m, LTC);  
 (N) Tectonic breccia with albitized fragments featuring polysynthetic twin albite crystals, overlaid by fissural carbonatization (SB-09-48m, LTC);  
 (O) Hydrothermal albite with chessboard-type twinning (SB-09-69m, LTC);  
 (P) Chloritized hydrothermal breccia with fragments of potassic rock (SB-08-119m, LTP);  
 (Q) Potassically altered tectonic breccia overlaid by fissural argilization (SB-09-69m, LTC);  
 (R) Quartz-feldspathic fault cataclasite, potassically altered and intersected by a quartz vein (SB-07-103m, LTC).

Abbreviations: Chl: chlorite; Ms: muscovite; Ser: sericite; Cb: carbonates; Qz: quartz; Fk: potassic feldspar; Ab: albite; Gal: Galena; Sph: Sphalerite; CCp: Chalcopyrite; Bn: Bornite; Gp: Gypsum; Py: Pyrite; LTP: transmitted light, parallel polarizers; LTC: transmitted light, crossed polarizers; LRP: reflected light, parallel polarizers.